

SIMULATING THE OPENING OF FUSIBLE-LINK- ACTUATED FIRE VENTS

by

Leonard Y. Cooper
Building and Fire Research Laboratory
National Institute of Standards and Technology
Gaithersburg, MD 20899 USA

Reprinted from the Fire Safety Journal, Vol. 34, No. 3, 219-255, April 2000.

NOTE: This paper is a contribution of the National Institute of Standards and Technology and is not subject to copyright.



NIST

National Institute of Standards and Technology
Technology Administration, U.S. Department of Commerce

Simulating the opening of fusible-link-actuated fire vents

Leonard Y. Cooper*

Building and Fire Research Laboratory, National Institute of Standards and Technology, Gaithersburg, MD 20899, USA

Received 3 November 1998; received in revised form 24 August 1999; accepted 2 September 1999

Abstract

Model equations, suitable for general use in compartment fire models, are developed to simulate the thermal response to arbitrary fire environments of fusible-link-activated automatic fire vents. The method of analysis, which focused on a prototype three-element link–mount design, can be extended to arbitrary multiple-element link mounts, including single-element simply supported links. A method was developed to determine the values of the set of parameters that characterize a particular multiple link–mount design. This involves: (1) the measured time-dependent thermal response of the link–mount design to exposure in a plunge test, the type of test used to characterize the thermal response of sprinkler links; and (2) an analytic means of determining values of the design parameters that yield an optimum fit between a solution to the model equations and the temperature data. The method takes account of the pre-fusing solder-melting phase of fusible-link response. The latter was shown to be very important for the link design used in this study. The method was carried out successfully for four plunge tests involving three link–mount systems and one or two system/flow orientations. The resulting system parameters and model equations were used in a successful simulation of vent actuation in a real, large-scale, fire scenario. Published by Elsevier Science Ltd.

1. Automatic vent opening devices: fusible links and drop-out vents

Ceiling-deployed fire vents are one traditional means of venting smoke during fires. Although many possible automatic or manual strategies for the opening of vents are

* Fax: 001-410-737-8688. Now at Hughes Associates, Inc., Baltimore MD, USA.
E-mail address: lcooper@haifire.com (L.Y. Cooper).

Nomenclature

$A_{\text{CONV},i}$	area of element i for convective heat transfer
C_{ij}	Eq. (14)
C'_{ij}	coefficient for conductive heat transfer from elements i to j
c_i	specific heat of element i
c_{MELT}	effective c_1 during solder melt phase
$F_{\text{RAD},i}$	Eq. (12)
$F_{\text{RAD},i,\text{PLUNGE}}$	$F_{\text{RAD},i}$ in a plunge test, Eq. (18)
G	Eq. (20)
h_i	average heat transfer coefficient of element i
k_{AIR}	thermal conductivity of air
$L_{\text{CONV},i}$	characteristic length of element i
L_{MELT}	solder's latent heat of melting
m_i	mass of element i
m_{MELT}	mass of melted solder needed to fuse the link
N_F	number of times data acquired in plunge test, up to t_{FUSE}
N_M	number of times data acquired in plunge test, up to t_{MELT}
Nu_i	Nusselt number of element i
\dot{Q}_{FIRE}	energy release rate of the fire
$\dot{Q}_{\text{RAD},i}$	Eq. (9)
$\dot{Q}_{\text{RADFIRE},i}$	Eq. (9)
$\dot{q}''_{\text{CONV},i}$	flux of convective heat transfer to element i
$\dot{q}''_{\text{RAD},i}$	flux of radiative heat transfer to element i
$\dot{q}''_{\text{RADFIRE}}$	flux of radiative heat transfer from the fire to a target
$\dot{q}''_{\text{RADFIRE},i}$	flux of radiative heat transfer from the fire to element i
R	radius from fire to target
Re_i	Reynolds number of element i flow
RTI	response time index
RTI_i	RTI of element i
RTI_{MELT}	RTI_1 during solder melt phase
r	radial distance to link-mount assembly
T_{AMB}	ambient temperature
T_{BASE}	temperature of the base of a sprinkler
T_{CEIL}	temperature of ceiling
$T_{\text{EXP},i}$	experimentally measured value of T_i
T_{FUSE}	fuse temperature of the link
T_G	gas temperature
T_{G-1}	Eq. (3)
T_{LINK}	link temperature
T_{MELT}	T when a plateau in T is indicated
T_{WALL}	wall temperature in plunge test
T_i	temperature of element i

t	time
t_j	t when data is acquired, $j = 1, N_F$
t_{FUSE}	t when $T_1 = T_{FUSE}$
t_{MELT}	t when a plateau in T_{LINK} is indicated
u	gas velocity
u_{CR}	a critical value of u
ΔT_{MELT}	Eq. (25)
ϵ	emissivity
ϵ_i	ϵ of element i
$\epsilon_{CEIL}, \epsilon_{FLOOR}$	ϵ of element i , ceiling, floor
ϵ_{WALL}	ϵ of wall in plunge test
A_i	Eq. (19)
λ_{RAD}	fraction of \dot{Q}_{FIRE} radiated to far field
ν_{AIR}	kinematic viscosity of air
σ	Stefan Boltzman constant
τ_i	Eq. (11)
<i>Subscripts</i>	
i	index of element i ; $i = 1, 2, 3$ refers to the link, tab, and bar, respectively

possible, a common strategy involves automatic actuation by use of a thermally sensitive device, deployed near the ceiling of the facility, in the immediate vicinity of the vent itself. Two typical devices are offered by vent manufacturers, the fusible link and the “device” of the drop-out vent.

In the case of the fusible link, a spring-loaded mechanism is designed to open the vent when restraint hardware, which includes the fusible link, is ruptured. In the event of a fire, the high-temperature smoke/fire gases rise to the ceiling of the protected facility, turn and flow across the ceiling and past the near-ceiling-deployed link, and heat it by forced convection. If the link temperature rises to its fuse temperature, T_{FUSE} , the solder that joins two bonded parts of the link melts. As a result, the link and, therefore, the vent-opening restraint hardware ruptures, and the vent opens.

The drop-out-type vent “device” involves a vent frame, mounted in the ceiling of the protected facility, whose opening is covered by a vent “dome”. The dome is formed from a plastic sheet, and is designed to soften, shrink, and drop out of the frame when heated to a sufficiently high temperature. The dropping-away action leads to the open-vent configuration. As in the case of the fusible link, the heating of the vent dome is primarily by convective heat transfer from the high-temperature smoke/fire gases that flow across the ceiling and across the lower surface of the vent-dome plastic. This work does not address further the subject of drop-out vent actuation.

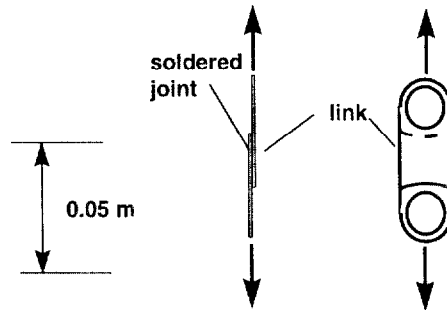


Fig. 1. The simply supported fusible link.

2. The objective of this work

The focus of this work is on vent system designs that depend on fusible links for their actuation. The objective is to develop a general mathematical model to simulate the action of fusible-link-actuated ceiling vents, where the model is suitable for general use in compartment fire models.

3. Simulating the thermal response of simply supported fusible links

Fig. 1 illustrates a typical fusible link design used in fire vents. This involves two pieces of steel, each with characteristic dimension of a few cm, joined by a solder connection over an area of a few cm^2 . The link is rated by the manufacturer according to the temperature at which the solder melts, T_{FUSE} . Commonly ratings are 74°C and 141°C .

As seen in Fig. 1, there is a hole at each end of the link. The ends of steel cabling are typically passed through these, and the cabling and link become an integral part of the above-mentioned vent-opening restraint. This kind of link-mount design will be referred to here as the *simply supported* link design.

The traditional method of predicting the thermal response of a simply supported link simply assumes that convective heating of the link dominates the heat transfer process. In particular, it is assumed that insignificant thermal contact with the cable connections at each end of the link leads to negligible conductive link-to-cable heat transfer, and that radiation heat transfer exchanges with the link do not play a significant role.

The traditional method by which the thermal response of simply supported links are simulated is the same as the original method used for the thermal response of fusible-link-actuated sprinklers [1–3], where conduction losses from the link to the base of the sprinkler were neglected. As in the case of sprinklers, the measured value of the link's response time index (RTI) [4] and T_{FUSE} are required to implement the

method. With known values of time-dependent gas flow speed and temperature local to the link, $u(t)$ and $T_G(t)$, respectively, the temperature of the link, $T_{\text{LINK}}(t)$, initially at the ambient temperature, T_{AMB} , can be obtained from the solution to

$$dT_{\text{LINK}}/dt = (T_G - T_{\text{LINK}})u^{1/2}/RTI \quad T_{\text{LINK}}(t = 0) = T_{\text{AMB}}, \quad (1)$$

up to time t_{FUSE} , when $T = T_{\text{FUSE}}$. In fire modeling applications, Eq. (1) is often used to simulate the response of both sprinkler and vent links (see, e.g., Refs. [5,6]).

4. Vent designs involving complex link mounts

Automatic vent designs can incorporate the action of Fig. 1-type fusible links that are not simply supported, and that cannot be expected to be simulated by Eq. (1). This is so, for example, in the case of the vent design used in large-scale tests conducted by Underwriters Laboratories (UL) for the National Fire Protection Research Foundation (NFPRF) [7–9], to investigate the interaction of sprinklers, vents, and draft curtains in industrial fires, and for Industrial Risk Insurers and Conspec Systems, Inc. [10], to investigate the relative sensitivity of roof-mounted heat and smoke vents. As will be presented below, the latter vent is designed with Fig. 1-type fusible link with one end simply supported and the other end welded and bolted to the steel frame of the vent.

An important aspect of the NFPRF-sponsored tests was the application by NIST of a computer fire model that uses a computational fluid dynamics (CFD) methodology based on large eddy simulation (LES) analysis [9]. The goal of the present work is the development of mathematical models of fire vent actuation that can be readily adapted by both CFD and zone-type compartment fire models.

A typical fire scenario in the NIST/NFPRF Research Program, including a sketch of the vents used (1.2 m × 2.4 m), is depicted in Fig. 2. As can be seen in this figure and in Fig. 3, the link is part of a three-element assembly, around which flows the elevated temperature gases of the fire-plume-driven ceiling jet. The assembly includes a 1.2 m-long structural steel “L”-bar (0.076 m × 0.102 m × 0.0048 m thick) that spans the vent frame, a steel tab welded to the center of the bar, and the link itself, bolted to the tab. Above the link and connected to it is a cable connected to the vent-opening mechanism. In the usual way, fusion of the link leads to opening of the vent.

In this vent design, heat transfer to each of the elements, the bar, the tab, and the link itself, of the three-element link-mount assembly plays a significant role in the thermal response of the vent-actuating fusible link. The next section develops a set of model equations to simulate the thermal response of the three-element mount. This would be used to predict fusing of the link and actuation of the vent for arbitrary fire scenarios. The equation set is designed to be versatile, in the sense that it can also be used to simulate the thermal response of fusible links implemented in other relatively-complicated link-mount configurations, and even in the simply-supported configuration.

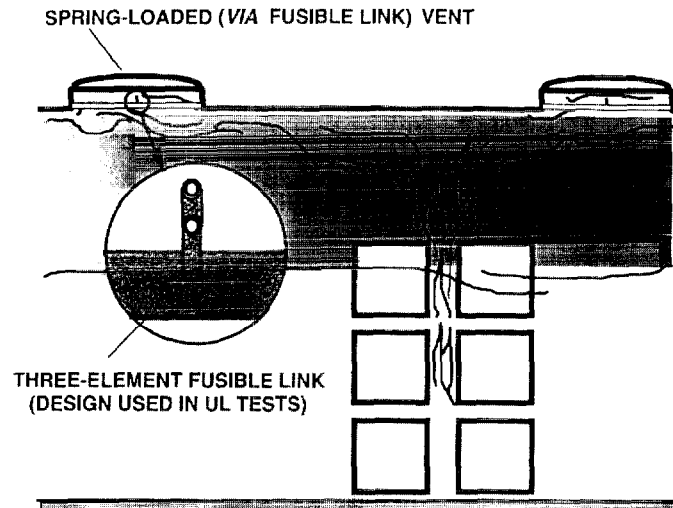


Fig. 2. A typical fire scenario in the NFPRF program [9], including a sketch of the vents with the three-element link-mount.

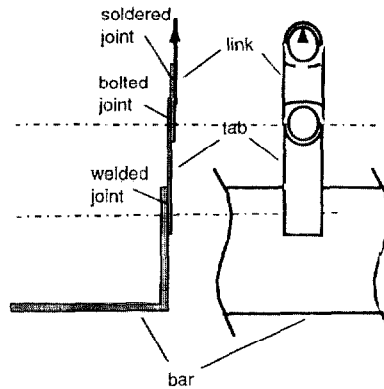


Fig. 3. The three-element link-mount assembly.

5. Simulating the thermal response of the three-element link-mount assembly

5.1. General comments

Corresponding to the three-elements link-mount assembly of Fig. 2, the mass, effective specific heat, and temperature of the bar, the tab, and the link, are designated as m_3, c_3, T_3 ; m_2, c_2, T_2 ; and m_1, c_1, T_1 , respectively. The elements are assumed to

Table 1
Some properties of air at standard pressure [12]

T_{G-i} (°C)	$k_{\text{AIR}}(T_{G-i})$ (W/(mK))	$\nu_{\text{AIR}}(T_{G-i})$ (m ² /s)	$k_{\text{AIR}}(T_{G-i})/\nu_{\text{AIR}}^{1/2}(T_{G-i})$ (W s ^{1/2} /(m ² K))
20	0.0251	15.7×10^{-6}	6.33
100	0.0307	23.6×10^{-6}	6.32
200	0.0370	35.5×10^{-6}	6.21
300	0.0429	49.2×10^{-6}	6.12
400	0.0485	64.6×10^{-6}	6.03
500	0.0540	81.0×10^{-6}	6.00

be physically small enough and close enough to each other that, in estimating the convective heat transfer, the instantaneous free-field gas flow local to each of them can be assumed to be spatially uniform, at the same temperature and speed, T_G and u , respectively.

5.2. Convective heat transfer to the elements

Relative to the gas flow over element i , the Reynolds number is

$$\text{Re}_i = uL_{\text{CONV},i}/\nu_{\text{AIR}}(T_{G-i}), \quad (2)$$

where u and T_G are the speed and temperature of the gas, $L_{\text{CONV},i}$ is a characteristic length of element i relative to estimates of gas-to-element convective heat transfer, and $\nu_{\text{AIR}}(T_{G-i})$ is the kinematic viscosity of air at temperature

$$T_{G-i} \equiv (T_G + T_i)/2. \quad (3)$$

The Re_i 's for fire scenarios and element geometries of interest here are expected to fall within the approximate range 100–5000. Using a result for the average rate of heat transfer to a circular cylinder in a crossflow of air, it is reasonable to estimate the individual average transfer coefficients, h_i from [11] where

$$\text{Nu}_i \equiv h_i L_{\text{CONV},i}/k_{\text{AIR}}(T_{G-i}) = 0.48(\text{Re}_i)^{1/2}, \quad (4)$$

where $k_{\text{AIR}}(T_{G-i})$ is the thermal conductivity of air. Then, using Eqs. (2) and (4) leads to

$$h_i = 0.48(u/L_{\text{CONV},i})^{1/2} k_{\text{AIR}}(T_{G-i})/\nu_{\text{AIR}}^{1/2}(T_{G-i}). \quad (5)$$

As can be seen in Table 1, and consistent with Refs. [1,2]

$$\text{for } 20^\circ\text{C} < T_{G-i} < 500^\circ\text{C}: \quad (6)$$

$$k_{\text{AIR}}(T_{G-i})/\nu_{\text{AIR}}^{1/2}(T_{G-i}) = 6.16(1 \pm 0.03) \text{ W s}^{1/2}/\text{m}^2 \text{ K}.$$

Therefore, from Eq. (5), h_i can be reasonably approximated as

$$\begin{aligned} h_i &= 0.48u^{1/2}L_{\text{CONV},i}^{-1/2}k_{\text{AIR}}(T_{G-i})/\nu_{\text{AIR}}^{1/2}(T_{G-i}) \\ &\approx 2.96(u/L_{\text{CONV},i})^{1/2} [\text{W s}^{1/2}/(\text{m}^2 \text{ K})]. \end{aligned} \quad (7)$$

5.3. Radiative heat transfer to the elements

In existing fire models, the effect of radiation heating on the thermal response of fusible links in fire environments is not included. This is true in the case of links used to control both vent or sprinkler actuation. Yet, in a proper analysis of link thermal response the effect of radiation may not be negligible. While the radiation effect does indeed seem to be negligible in the case of the relatively small links typically used in sprinkler design, in the case of the relatively large-component link–mount assemblies used in vent designs, the effect of radiation on link response may be significant. For example, consider the three-element link–mount of Fig. 2 where the width of the link is $L_{\text{CONV},3} = 0.019$ m and the temperature of fusing is, $T_{\text{FUSE}} = 74^\circ\text{C}$. At an instant of time during a fire scenario, make the following assumptions: $T_{\text{LINK}} = T_1 = 70^\circ\text{C}$; $u = 4.0$ m/s and $T_G = 110^\circ\text{C}$ near the link; throughout the space of fire origin the gas is still relatively transparent and does not participate in any significant radiative heat transfer exchange; the link exchanges radiation with far field surfaces which are still at near-ambient temperature, $T_{\text{AMB}} = 20^\circ\text{C}$; effective emissivity of the link and all far-field surfaces, ϵ , are 0.9. Then, using Eq. (7), the instantaneous components of convective and radiative heat transfer to the link are

$$\begin{aligned} \dot{q}_{\text{CONV},1}'' &= h_1(T_G - T_1) = 1.72 \times 10^3 \text{ W/m}^2; \\ \dot{q}_{\text{RAD},1}'' &= \sigma(T_{\text{AMB}}^4 - T_1^4)/(2\epsilon - 1) = -0.30 \times 10^3 \text{ W/m}^2, \end{aligned}$$

where $\sigma = 5.67 \times 10^{-8}$ W/(m² K⁴) is the Stefan–Boltzman constant.

In the above example, it is seen that the magnitude of radiation cooling of the link to the far field is relatively small compared to that of convective heating, and the traditional neglect of radiation in an engineering calculation of link response may be justified. However, if a higher- T_{FUSE} link is used, and if, say, $T_{\text{LINK}} = T_1 = 90^\circ\text{C}$ and all of the other above parameters are the same, then

$$\dot{q}_{\text{CONV},1}'' = 0.86 \times 10^3 \text{ W/m}^2, \quad \dot{q}_{\text{RAD},1}'' = -0.46 \times 10^3 \text{ W/m}^2.$$

In the latter case, an analysis that neglects radiation compared to convection would be unacceptable. Also, in the case of the physically larger bar, the third element of the three-element link–mount, $L_{\text{CONV},3} \approx 0.076$ m $>$ $L_{\text{CONV},1}$. Therefore, From Eq. (7) it is clear that h_3 will be significantly smaller than h_1 , and it can be anticipated that, compared to convection, radiative heating of this bar element will always be important.

Finally, in simulating the thermal response of the three link–mount elements during a fire scenario, direct radiation from the combustion zone will lead to an additional component of heat transfer. This can lead to significant modifications in the response of all the elements, i.e., even for the physically small link. For example, for a fire with total energy release rate $\dot{Q}_{\text{FIRE}} = 10$ MW, if 35% of the energy released in the combustion zone is radiated away as from a point source of radiation, then the rate of radiation flux incident on the projection of a target area (e.g., the surface of the fusible link) normal to a radius from the source, where the target is $R = 10$ m from the fire, will be

$$\dot{q}_{\text{ADIFIRE}}'' = 0.35\dot{Q}_{\text{FIRE}}/(4\pi R^2) = 2.78 \times 10^3 \text{ W/m}^2.$$

To estimate the significance of this $\dot{q}_{\text{RADFIRE}}''$ relative to $\dot{q}_{\text{CONV},1}$ in the present example, assume a ceiling height of 7.5 m, i.e., the link is near the ceiling, at a radius of 6.6 m from the point of plume/ceiling impingement. Then, at the radial location of the link and for an expansive ceiling with a thin upper layer, the fire model *LAVENT* [6,13,14] was used to estimate the maximum ceiling jet velocity and temperature, which were found to be $u = 2.1$ m/s and $T_G = 246^\circ\text{C}$, respectively. Assuming again that $T_{\text{LINK}} = T_1 = 70^\circ\text{C}$, Eq. (7) now leads to the result

$$\dot{q}_{\text{CONV},1}'' = h_1(T_G - T_1) = 2.10 \times 10^3 \text{ W/m}^2.$$

Thus, in this example, it is concluded that direct radiative heat transfer from the fire to the link, being comparable to convective heat transfer, must be taken into account in an analysis of the thermal response of the link. It therefore seems that, in general, $\dot{q}_{\text{RADFIRE}}''$ should be taken into account in engineering analyses of fusible-link response. Indeed, except in the case of particularly small-dimension fusible links where pre-actuation exposure to direct fire radiation is not particularly intense, the latter radiation component should also be accounted for when modeling the thermal response of the fusible links used to actuate sprinklers.

In view of the last observation, it is noteworthy that in real fire scenarios, and for the purpose of making a priori estimates of $\dot{q}_{\text{RADFIRE}}''$, it is typically impossible to estimate accurately the effective location of the combustion zone, both in terms of assigning radial distance from and orientation to the radiated surface of a target fusible link or other link-mount elements. Since $\dot{q}_{\text{RADFIRE}}''$ is strongly dependent on the latter two variables, the situation for accurate a priori simulation estimates of link thermal response is particularly problematic. Also, to the extent that (in the relatively early time intervals of interest) the ceiling jet and the developing upper gas layer are not relatively transparent to relevant radiation wave lengths, the above radiative heat transfer estimates and the model equations to be developed below would have to be modified appropriately.

To include the effects of radiative heat transfer on element response, and with the latter observation in mind, model equations for $\dot{q}_{\text{RAD},i}''$ and $\dot{q}_{\text{RADFIRE}}''$ are constructed consistent with the following definition and assumptions:

Define $A_{\text{CONV},i}$ as the effective area for gas-to-element convective heat transfer to element i .

Prior to the time of link fusing, assume that the lower surfaces of the room of fire origin are still near T_{AMB} and that radiation, absorption, and emission of the upper gas layer and ceiling jet gases are negligible.

Regarding $\dot{q}_{\text{RAD},i}''$, assume half of $A_{\text{CONV},i}$, the “top” half, exchanges radiation with a far field having temperature and effective emissivity identical to that of the nearby ceiling surface of the room, T_{CEIL} and ϵ_{CEIL} , respectively. Assume the other half of $A_{\text{CONV},i}$, the “bottom” half, exchanges radiation with a far field having temperature and effective emissivity identical to that of the floor surface of the room or of the “facing” surfaces of the room contents, T_{AMB} and ϵ_{FLOOR} , respectively, i.e., for times of interest, the floor or facing content’s surfaces are assumed to still be close to ambient temperature.

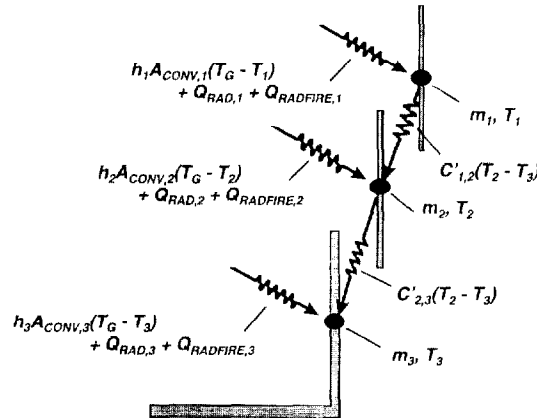


Fig. 4. Components of heat transfer to the three elements of the link–mount assembly of Fig. 3.

Regarding $\dot{q}_{\text{RADFIRE},i}$, assume that the radiant energy from the fire's combustion zone, effectively a point source at elevation y_{FIRE} above the floor, radiates isotropically at a rate $\lambda_{\text{RAD}}\dot{Q}_{\text{FIRE}}$, where \dot{Q}_{FIRE} is the total energy release rate of the fire and λ_{RAD} is the fraction of this radiated to the far field, of the order of 0.35 for typical hazardous fires [6].

Assume half of $A_{\text{CONV},i}$ is exposed to direct radiation from the fire, i.e., one side of the element is illuminated by the combustion zone and the other side is shaded. Assume further, that the projection of this exposed surface on a surface normal to a radial vector from the fire source is half of its full area.

5.4. Model equations for the thermal response of the fusible link

From the onset of a fire scenario, $t = 0$, when all T_i are at T_{AMB} , to the time of link fusing, $t = t_{\text{FUSE}}$ when $T_1 = T_{\text{FUSE}}$, and consistent with the above definitions and assumptions as depicted in Fig. 4, energy conservation for the three elements of the link–mount leads to

For $0 \leq t \leq t_{\text{FUSE}}$ = specified:

$$\begin{aligned} m_1 c_1 \, dT_1/dt &= h_1 A_{\text{CONV},1}(T_G - T_1) - C'_{12}(T_1 - T_2) + \dot{Q}_{\text{RAD},1} + \dot{Q}_{\text{RADFIRE},1}, \\ m_2 c_2 \, dT_2/dt &= h_2 A_{\text{CONV},2}(T_G - T_2) + C'_{12}(T_1 - T_2) - C'_{23}(T_2 - T_3) \\ &\quad + \dot{Q}_{\text{RAD},2} + \dot{Q}_{\text{RADFIRE},2}, \end{aligned} \quad (8)$$

$$\begin{aligned} m_3 c_3 \, dT_3/dt &= h_3 A_{\text{CONV},3}(T_G - T_3) + C'_{23}(T_2 - T_3) + \dot{Q}_{\text{RAD},3} + \dot{Q}_{\text{RADFIRE},3}, \\ \dot{Q}_{\text{RAD},i} &= (A_{\text{CONV},i}/2)\sigma[(T_{\text{CEIL}}^4 - T_i^4)/(1/\epsilon_{\text{CEIL}} + 1/\epsilon_i - 1) \\ &\quad + (T_{\text{AMB}}^4 - T_i^4)/(1/\epsilon_{\text{FLOOR}} + 1/\epsilon_i - 1)], \end{aligned} \quad (9)$$

$$\dot{Q}_{\text{RADFIRE},i} = (A_{\text{CONV},i}/4)\lambda_{\text{RAD}}\dot{Q}_{\text{FIRE}}/\{4\pi[r^2 + (y_{\text{CEIL}} - y_{\text{FIRE}})^2]\},$$

where

$$T_i(t = 0) = T_{\text{AMB}}, \quad i = 1, 2, \text{ or } 3, \quad (10)$$

$\dot{Q}_{\text{FIRE}} = \dot{Q}_{\text{FIRE}}(t)$, $T_G = T_G(t)$, $u = u(t)$, and $T_{\text{CEIL}} = T_{\text{CEIL}}(t)$ are specified.

In Eqs. (8), the $h_i A_{\text{CONV},i}(T_G - T_i)$ terms represent the rate of convective heat transfer from the gas to element i and the $C'_{ij}(T_i - T_j)$ terms represent the rate of conductive heat transfer from element i to element j . In Eqs. (8) and (9), the $\dot{Q}_{\text{RAD},i}$ and $\dot{Q}_{\text{RADFIRE},i}$ terms are the respective total rates of heat transfer to element i from radiation exchanges with the bounding surface of the enclosure and from direct radiation from the fire; ϵ_i is the effective emittance/absorptance of the assumed-grey surfaces of element i , y_{CEIL} is the elevation of the ceiling above the floor; and r is the radial distance of the link-mount assembly from the point of fire plume/ceiling impingement.

Following and extending nomenclature of Refs. [15,16], define τ_i and rewrite Eqs. (8) as

$$\tau_i = m_i c_i / (h_i A_{\text{CONV},i}), \quad i = 1, 2, \text{ or } 3, \quad (11)$$

$$dT_1/dt = (T_G - T_1)/\tau_1 - C'_{12}(T_1 - T_2)/(m_1 c_1) + F_{\text{RAD},1},$$

$$dT_2/dt = (T_G - T_2)/\tau_2 + C'_{12}(T_1 - T_2)/(m_2 c_2) - C'_{23}(T_2 - T_3)/(m_2 c_2) + F_{\text{RAD},2}, \quad (8')$$

$$dT_3/dt = (T_G - T_3)/\tau_3 + C'_{23}(T_2 - T_3)/(m_3 c_3) + F_{\text{RAD},3},$$

where the $F_{\text{RAD},i}$, which include all effects of radiation heat transfer on element i , are

$$F_{\text{RAD},i} = F_{\text{RAD},i}(T_i^4; \text{specified parameters}) = (\dot{Q}_{\text{RAD},i} + \dot{Q}_{\text{RADFIRE},i})/(m_i c_i). \quad (12)$$

Using Eq. (7) in Eq. (11) leads to

$$\tau_i u^{1/2} \equiv \text{RTI}_i \approx [(L_{\text{CONV},i}^{1/2} m_i c_i / A_{\text{CONV},i}) / 2.96] [\text{m}^2 \text{K} / (\text{W s}^{1/2})]. \quad (13)$$

As can be seen, the right-hand side of the above equation is a constant determined by mechanical/thermal and geometric properties of element i . For the fusible link, element 1, is identical to the RTI of the link as defined in Refs. [1,2,15,16]. Here, the right-hand side of Eq. (13) is designated RTI_i , or the RTI of element i .

Using Eq. (13) in Eqs. (8') leads to

For $0 \leq t \leq t_{\text{FUSE}}$ = specified:

$$dT_1/dt = [T_G - (1 + C_{12}/u^{1/2})T_1 + (C_{12}/u^{1/2})T_2]u^{1/2}/\text{RTI}_1 + F_{\text{RAD},1},$$

$$dT_2/dt = [T_G - (1 + C_{21}/u^{1/2} + C_{23}/u^{1/2})T_2 + (C_{21}/u^{1/2})T_1 + (C_{23}/u^{1/2})T_3]u^{1/2}/\text{RTI}_2 + F_{\text{RAD},2}, \quad (8'')$$

$$dT_3/dt = [T_G - (1 + C_{32}/u^{1/2})T_3 + (C_{32}/u^{1/2})T_2]u^{1/2}/\text{RTI}_3 + F_{\text{RAD},3},$$

subject to the conditions of Eq. (10),

where

$$\begin{aligned}
 C_{12}/C'_{12}RTI_1/(m_1c_1) &= C'_{12}[(L_{CONV,1}^{1/2}/A_{CONV,1})/2.96] [m^2 K/(W s^{1/2})], \\
 C_{21}/C'_{12}RTI_2/(m_2c_2) &= C'_{12}[(L_{CONV,2}^{1/2}/A_{CONV,2})/2.96] [m^2 K/(W s^{1/2})], \\
 C_{23}/C'_{23}RTI_2/(m_2c_2) &= C'_{23}[(L_{CONV,2}^{1/2}/A_{CONV,2})/2.96] [m^2 K/(W s^{1/2})], \\
 C_{32}/C'_{23}RTI_3/(m_3c_3) &= C'_{23}[(L_{CONV,3}^{1/2}/A_{CONV,3})/2.96] [m^2 K/(W s^{1/2})].
 \end{aligned} \tag{14}$$

Also, from Eqs. (14)

$$\begin{aligned}
 C_{21} &= C_{12}(m_1c_1RTI_2)/(m_2c_2RTI_1), \\
 C_{32} &= C_{23}(m_2c_2RTI_3)/(m_3c_3RTI_2).
 \end{aligned} \tag{15}$$

Note that m_i and c_i can be easily obtained. Therefore, it is assumed they are known and specified. Then, corresponding to a set of five system parameters RTI_1 , RTI_2 , RTI_3 , C_{12} , and C_{23} , to be determined, the values of C_{21} and C_{32} are obtained directly from Eqs. (15).

6. Determining the thermal properties of the link–mount assembly

6.1. General considerations

The solution to the problem of Eqs. (8'') and (10) would provide a prediction of the thermal response of the link–mount assembly when it is exposed to a specified fire environment and corresponding local flow. For a vent located at a particular location relative to a fire scenario of interest, and with known local values of $T_G(t)$ and $u(t)$ (e.g., determined from a fire model simulation), the solution would yield the $T_i(t)$. Of interest here would be the solution for $T_1(t)$, the temperature of the fusible link itself, and, in particular, a determination of t_{FUSE} , the time when it fuses and when the vent opens.

To fully define the problem for a particular vent design, it is necessary to determine the thermal properties of the link–mount assembly, i.e., the five-system parameters RTI_1 , RTI_2 , RTI_3 , C_{12} , and C_{23} . This section addresses means of determining these parameters. This will use a combined-experimental/analytic method, where the experimental aspect involves use of the plunge test [1,2,15], originally developed to determine the RTI for sprinkler links.

6.2. The plunge test

The plunge test is a wind-tunnel test where, in its designed application, a sprinkler head, with its actuating link–mount assembly (T_{FUSE} of the link is known), all at initially ambient temperature, is inserted (i.e., “plunged”) into an air stream of specified constant temperature, $T_G > T_{FUSE}$, and specified constant flow speed, u . An original purpose of the plunge test was to determine the thermal characteristics of different sprinkler designs, so that sprinkler actuation, i.e., fusing of the link, could be predicted when the sprinkler head is exposed to an arbitrary, specified, time-dependent fire-environment.

Note that the currently accepted model equation for sprinkler link thermal response (see, e.g., Refs. [15,16]), which includes the effect of conduction loss from the link to the sprinkler base, is a special case of Eqs. (8'') and (10), where, as in the present analysis, T_1 is the temperature of the link, but where T_2 is the temperature of the base of the sprinkler assembly, assumed to be at a known constant temperature, usually taken to be T_{AMB} ; C_{12} characterizes the conduction path between the link and the sprinkler base; radiation effects are ignored, and only the first of Eqs. (8'') is applicable. Thus, the traditional model equations for the response of a sprinkler link exposed to an arbitrary fire environment are

For $0 \leq t \leq t_{FUSE}$ = specified:

$$dT_1/dt = [T_G - (1 + C_{12}/u^{1/2})T_1 + (C_{12}/u^{1/2})T_2]u^{1/2}/RTI_1 \quad (8''')$$

where

$$T_1(t=0) = T_{AMB} \quad \text{and} \quad T_G = T_G(t), u = u(t) \text{ are specified.} \quad (10')$$

In the case of a constant-velocity/temperature plunge-test exposure, and neglecting effects of radiation, the general solution to the above for $T_1(t)$ is readily determined (see Eq. (21) of Ref. [15]). In particular, at $t = t_{FUSE}$

$$RTI_1 = -t_{FUSE}u^{1/2}(1 + C_{12}/u^{1/2})/\ln[1 - (T_{FUSE} - T_{AMB}) \times (1 + C_{12}/u^{1/2})/(T_G - T_{AMB})]. \quad (16)$$

Thus, if C_{12} is known, the RTI_1 of the sprinkler link can be determined from a single plunge test.

As discussed in Ref. [15], C_{12} can be determined from additional application of the plunge test apparatus. The idea is to expose the sprinkler head to series of quasi-steady exposures at a fixed T_G . The exposures involve an initial value of u that is less than required to affect fusing of the link. A steady-state condition is established where the conductive heat transfer from the link to the cool sprinkler base is large enough, and the rate of heat transfer from the relatively low-speed gas to the link is small enough to maintain the link at a temperature less than T_{FUSE} . Then u is increased in small steps. After allowing the system enough time between steps to reach a quasi-steady state, with dT_1/dt effectively zero (in the tests of Ref. [15], an interval of 10 min was adequate), the value of T_{BASE} , the temperature of the base of the sprinkler, is recorded. Eventually, during one of these steps, the link will attain T_{FUSE} . Designate u for this step as the critical u , $u_{CR} = u_{CR}(T_G)$. Then, the steady version of the first of Eqs. (8'') leads to the desired objective

$$C_{12} = u_{CR}^{1/2}(T_G - T_{FUSE})/(T_{FUSE} - T_{BASE}) \quad (17)$$

(also see Eq. (25) of Ref. [15]), where, in these quasi-steady exposures, T_{BASE} may be measurably higher than T_{AMB} .

Having determined C_{12} from the latter test sequence, it can be used in Eq. (16), together with the previously measured plunge-test value of t_{FUSE} , to determine the desired value of RTI_1 . With the values of RTI_1 and C_{12} in hand, link response to any arbitrary, specified fire exposure can be determined from a solution to Eqs. (8''') and (10').

6.3. The plunge test and the link-mount assembly

As is the case for single sprinkler-head assemblies, the response to plunge test exposures of the more complex link-mount assembly of current interest can also be measured. However, while the above two-stage test approach (a single time-dependent exposure to link fusing, and a series of quasi-steady exposures) leads to a determination of RTI_1 and C_{12} , and a complete thermal characterization of the two-parameter sprinkler-head systems, this is not the case for the five-parameter link-mount assembly. Furthermore, because of the current concern that radiation effects may be important, even in the plunge test environment (i.e., radiation exchanges between the elements and the relatively high-temperature tunnel walls), the situation is complicated even farther. In short, an alternative method is required to determine, from measured time-dependent responses to plunge test exposures, the five system parameters of the link-mount assembly.

7. Modified equations for response under plunge test conditions

The problem of Eqs. (8'') and a simplified version of Eqs. (10) can be used to simulate the response of the link-mount assembly during a plunge test exposure if the radiation terms, $F_{RAD,i}$, as defined by Eqs. (9) and (12), are modified/reinterpreted. First, the non-operative direct-fire-radiation term, $\dot{Q}_{RADFIRE,i}$, is eliminated. Then, in $\dot{Q}_{RAD,i}$, the characteristics of the ceiling and the floor of the fire room are replaced by the corresponding characteristics of the inside wall in the test section of the tunnel, which surrounds the assembly. This leads to

$$\begin{aligned} F_{RAD,i} &= F_{RAD,i, PLUNGE} = (\dot{Q}_{RAD,i})/(m_i c_i) \\ &= A_{CONV,i} \sigma (T_{WALL}^4 - T_i^4) / [(1/\epsilon_{WALL} + 1/\epsilon_i - 1)(m_i c_i)]. \end{aligned} \quad (18)$$

This is used in Eqs. (8''), and the problem definition is completed with

$$T_i(t = 0) = T_{AMB}, \quad i = 1, 2, \text{ or } 3; \quad T_G, u, \text{ and } T_{WALL} \text{ are specified constants.} \quad (10'')$$

8. Determining the thermal properties of the link-mount assembly

8.1. An algorithm for determining the system parameters

Corresponding to the unknown RTI_i 's and the C_{ij} 's, of the link-mount assembly, define the five system parameters A_i by

$$\begin{aligned} A_1 &= T_G u^{1/2} / RTI_1, \quad A_2 = T_G u^{1/2} / RTI_2, \quad A_3 = T_g u^{1/2} / RTI_3, \\ A_4 &= (C_{12} / RTI_1), \quad A_5 = (C_{23} / RTI_2). \end{aligned} \quad (19)$$

For an arbitrary choice of the parameters, let $T_i(t; A_1, \dots, A_5)$ be the solution to Eqs. (8''), (18) and (10''), from $t = 0$ to $t = t_{\text{FUSE}}$. Such a solution can presumably be obtained by numerical integration.

Let the link-mount assembly be subjected to a plunge test and denote the experimental data for the variables $T_i(t)$ as $T_{\text{EXP},i}(t_j)$, $j = 1, N_F$, where N_F is the number of times that data were acquired up to t_{FUSE} .

Now consider the following problem:

Determine the values of A_k that minimize

$$G(A_k, T_{\text{EXP},i}(t_j)) = \sum_{i=1}^3 \sum_{j=1}^{N_i} [T_{\text{EXP},i}(t_j) - T_i(t_j; A_1, \dots, A_5)]^2. \quad (20)$$

It is now assumed that the set of A_k solutions to the above problem correspond to a best estimate of the desired thermal properties of the link-mount assembly. Thus, from Eqs. (19) the desired system parameters are obtained from

$$\text{RTI}_i = T_G u^{1/2} / A_i, i = 1, 3; C_{12} = T_G u^{1/2} (A_4 / A_1), C_{23} = T_g u^{1/2} A_5 / A_2. \quad (21)$$

Characterization of the system is completed by using Eq. (15) and the results of Eq. (21) to determine

$$C_{21} = T_g u^{1/2} (A_4 / A_2) (m_1 c_1) / (m_2 c_2), C_{32} = T_g u^{1/2} (A_5 / A_3) (m_2 c_2) / (m_3 c_3). \quad (22)$$

8.2. Implementing the least-squares curve fitting algorithm

An implementation of the above algorithm requires: plunge test data, $T_{\text{EXP},i}(t_j)$; numerical integration of the initial value problem of Eqs. (8''), (18) and (10'') necessary to compute $T_i(t; A_k)$ and $G(A_k, T_{\text{EXP},i}(t_j))$ of Eq. (20); and an algorithm and associated computer software to find the set of parameters that minimize the sum of squares of a set of non-linear functions of several variables.

In the carrying out the above, the numerical integration subroutine used was *ODEINT* from Ref. [17], and the minimization subroutine used was *SNLSIE* from Ref. [18].

9. Plunge tests on the link-mount assembly of Figs. 2 and 3 and on related link-mount assemblies

9.1. A modified short-bar link-mount test assembly

As mentioned, the bar element of the link-mount assembly is 1.2 m long, too long to be tested in the 0.20 m × 0.20 m test section of the plunge test apparatus. However, it is expected that somewhat away from its end mounts, the thermal response of this full-length bar to exposures of Fig. 2-type fire environments does not vary significantly along its length. It is also reasonable to expect that the thermal response to fire environments of a relatively short “free-end” segment of the bar (length of at least a few times the characteristic dimension of the bar’s section) would be substantially similar to that of the full-length bar.

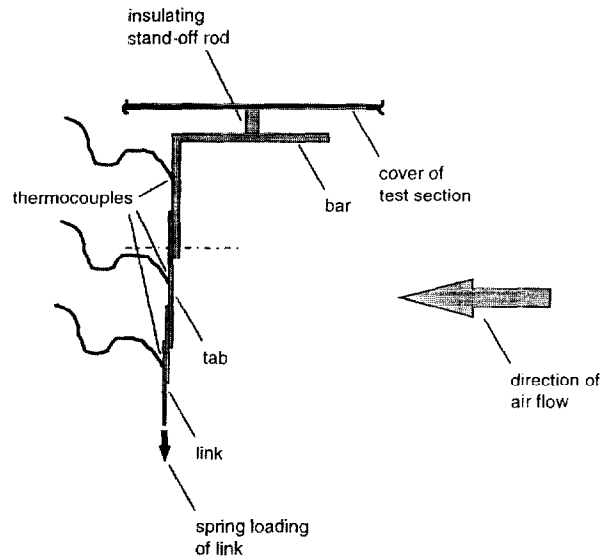


Fig. 5. The three-element link-mount assembly in the plunge test of test 1.

The above expectations are the basis for testing a modified Fig. 2-type three-element link assembly, with a shortened free-end bar element, and for assuming that its response in both uniform, steady, plunge-type flows and in time-dependent real fire environments will be substantially similar to that of a full-length-bar assembly. The length of the bar element of the tested assembly was 0.121 m. Except for the shortened length of the bar, the construction of the three-element link-mount test assembly, i.e., the tab and link elements and the means of element-to-element attachment, per Fig. 3, was identical to that found in the real vent hardware.

The fusible links used were all identical, as depicted in Figs. 1 and 3, with a rated fuse temperature of 74°C.

9.2. The test procedure and measurements

See Fig. 5. The test assembly was mounted via an insulating 0.010 m-diameter stand-off rod between the base of its bar element and a steel cover plate used to cover the opening of the test section. The design led to rigid test fixture with a 0.020 m stand-off distance between the bar base and the cover. In the test procedure, the tunnel, with covered ceiling test section opening, but without the test fixture, was brought up to the desired steady gas velocity and temperature; the inside wall temperature, continuously measured in the vicinity of the test section, was also at steady state. At the initiation of a test, the test section was opened, and the test assembly fixture was inserted upside-down into the test section. The insertion action took on the order of 1 s.

The temperature of each of the three elements was measured every 0.5 s with thermocouples peened to the element surface at the locations indicated in Fig. 5. T_{WALL} was measured in the immediate vicinity of the test section and T_{G} was measured upstream of the test section.

One test was carried out with the air flow normal to the length of the bar axis (as in Fig. 5) and one test with the air flow parallel to the bar axis.

A feature of the assembly/cover test fixture, indicated in Fig. 5, allowed for a constant 1.4 kg axial spring loading of the link, and for visual confirmation, outside the tunnel, of when the link fused. The time of link fusing could also be clearly distinguished by a significant subsequent increase of temperature of the link thermocouple which quickly approached the air flow temperature.

A test was terminated at $t = t_{\text{FUSE}}$.

9.3. Related link-mount assembly: three-element assembly with insulating connections

One test was carried out on a second three-element assembly, referred to here as the “element-isolated assembly”. This was identical to the three-element assembly of Fig. 3, except that it was fabricated so that the element-to-element thermal conduction paths are modified in such a way as to significantly reduce inter-element conduction, without modifying the basic gas-to-element convective heat transfer phenomena. In the assembly design, the link-to-tab and tab-to-bar joints involved insulating spacers fabricated from 0.0016 m-thick epoxy-resin-type circuit board material and fastened to the respective surfaces with a high-temperature adhesive.

The test on the element-isolated assembly was with the air flow parallel to the test assembly.

9.4. Related link-mount assembly: simply supported fusible link

A final test was carried out on a simply supported fusible link (see Fig. 1). As in the normal-flow test of Fig. 5, the surface of the link was normal to the flow, and it was instrumented with a thermocouple peened to the center of its rear surface. The test fixture provided spring loading of the link during the test and visual indication of link fusing.

9.5. Test conditions and test results

For all tests, thermostatic control of the gas flow temperature at 135°C led to measured values of $T_{\text{G}} = 134^{\circ}\text{C} \pm 1.0^{\circ}\text{C}$. Using previous calibrations of tunnel flow velocity vs. gas flow temperature, the tunnel fan speed control was set at a value corresponding to an average test flow velocity, $u = 2.5$ m/s.

Table 2 presents an overview of all tests, including: test conditions; the test results: T_{WALL} , $T_1(t = t_{\text{FUSE}})$, t_{FUSE} , N_{F} ; and reference to the figure numbers where the measured T_i are plotted. Also included in the table are t_{MELT} and N_{M} , to be defined below.

Table 2
Plunge test configurations, conditions, and results

Test no.	Configuration	Flow direction	T_{AMB}	T_G (°C ± 1°C)	T_{WALL}	T_i (t_{FUSE})	t_{FUSE} (s)	N_i	t_{MELT} (s)	N_M	Fig. no.
1	Full assembly	Normal	25	134	90	74	68.0	137	34.1	69	6
2	Full assembly	Parallel	24	134	97	74	63.0	127	34.5	70	7
3	Element-isolated assembly	Parallel	24	134	97	73	54.5	110	31.5	64	8
4	Simply supported link	Normal	24	133	100	74	53.5	108	25.0	50	9

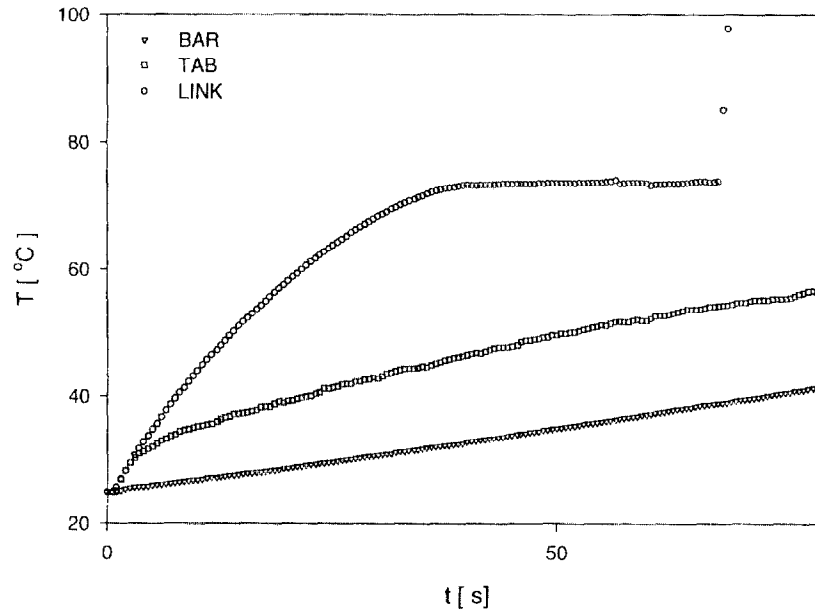


Fig. 6. Temperature data for the link-mount configuration and flow orientation of test 1 (see Table 2).

10. Overview of results

Main features of the test results are:

Within experimental accuracy the links used in each of the five tests fused at the specified device fuse temperature, $T_i(t_{FUSE})$, of 74°C.

Results of tests 1 and 2 indicated that orientation of the three-element assemble relative to flow direction does not have a significant effect on t_{FUSE} (68.0 and 63.0 s, respectively) or on the T_i (see Figs. 6 and 7, respectively).

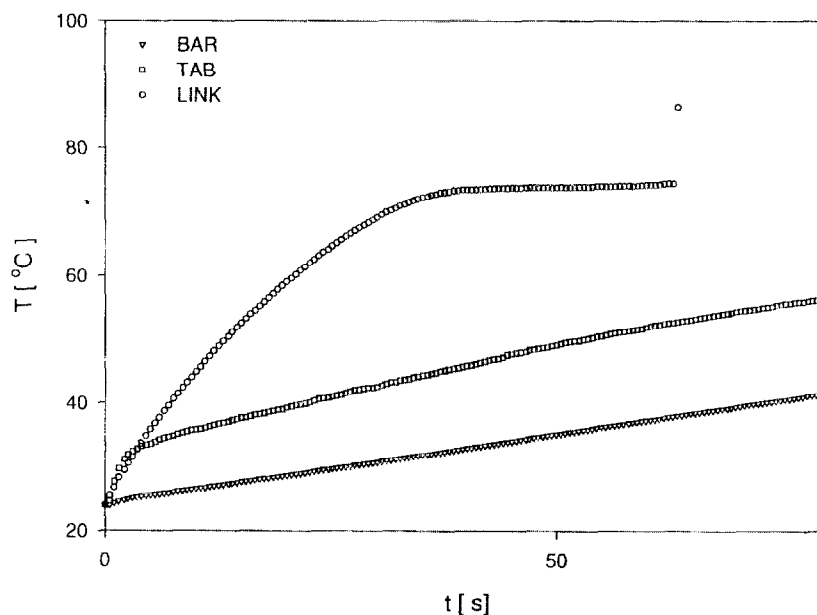


Fig. 7. Temperature data for the link–mount configuration and flow orientation of test 2 (see Table 2).

From Figs. 6–8, the effect of increasing element-to-element thermal isolation (compare the full assembly of tests 1 and 2 to the element-isolated assembly of test 3) is seen to have qualitatively modified element response. Initially, the temperature of both the bar, T_3 , and the tab, T_2 , in test 3 increased more rapidly than they had in tests 1 and 2, with T_2 greater than the temperature of the link, T_1 , until well into the test.

It is seen that the differences between t_{FUSE} for the full assembly in tests 1 and 2 (68.0 and 63.0 s, respectively) and t_{FUSE} for the simply supported link of test 4 (53.5 s) were 14.5 and 9.5 s, respectively, a reduction of 21 and 15%, respectively. Thus, in spite of the firm connection of the link to the relatively massive tab and bar in the three-element link mount assembly, t_{FUSE} for the full assembly is not increased significantly over that of the simply supported link.

In terms of a t_{FUSE} measure, the response of the link of the element-isolated assembly (54.5 s) in test 3 was very close to that of the simply supported link (53.5 s) of test 4.

For all tests, the T_1 histories of Figs. 6–9 indicate that the time interval over which link solder melting takes place, i.e., the interval when the link is maintained close to its fuse temperature, is a significant fraction of t_{FUSE} , of the order of 50%.

Relative to the success of the traditional RTI modeling concept, which neglects the time interval of solder melting compared to t_{FUSE} , the latter result is particularly significant. Thus, for the fusible link design tested here, the RTI model equation for the link, whether for a simply supported link, i.e., Eq. (8'''), or for the three-element link mount of current interest, i.e., the first of Eqs. (8''), or of Eqs. (8''), etc., is not adequate.

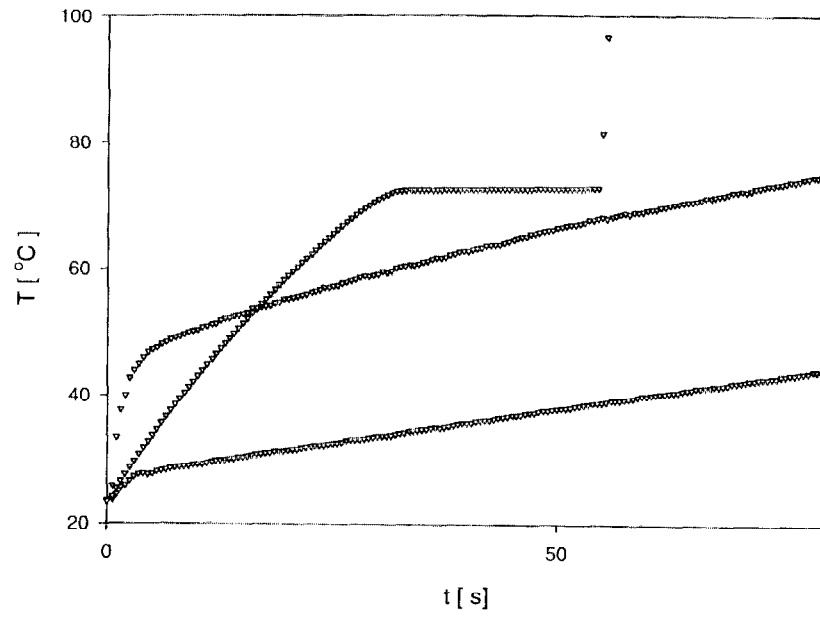


Fig. 8. Temperature data for the link-mount configuration and flow orientation of test 3 (see Table 2).

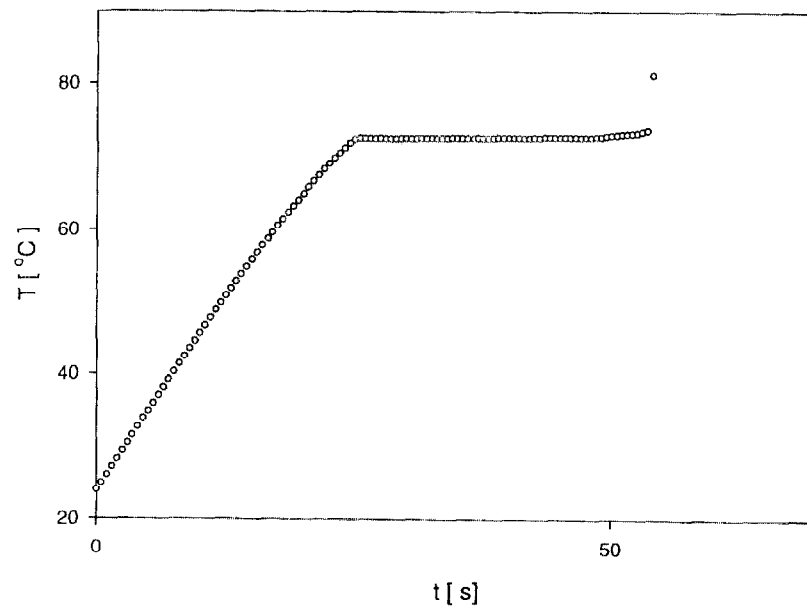


Fig. 9. Temperature data for the link-mount configuration and flow orientation of test 4 (see Table 2).

Rather, the model equations will have to be modified to take into account the phenomenon of solder melting and the extended time of nearly constant link temperature prior to link fusing.

Note that the latter effect of an extended interval of link solder melting has apparently not been observed in the thermal response of fusible links traditionally used in sprinkler design. Indeed, the Eq. (8'') model has proved to be very robust in the simulation of these devices.

11. Applying the least-squares curve fitting algorithm to determine system parameters

11.1. Two applications of the algorithm for each test

With the availability of the above T_i test data, it is possible to apply the above-proposed least-squares algorithm to determine the RTI_i and the C_{ij} parameters that define the thermal response characteristics of the three configurations: the full assembly (tests 1 and 2), the element isolated assembly (test 3) and the simply supported link (test 4). This will be done without regard for the above observation on the inadequacy of the model equations for T_1 . Thus, although it is now apparent that the previously adopted system of equations does not represent an optimum model for the T_i , it is still reasonable to use the experimental plunge test results and to determine those values of RTI_i and C_{ij} that optimize the system equations, Eqs. (8'') and (10'), according to the algorithm of Eq. (20), etc. Later, overall model equations will be improved, and corresponding system parameters will be determined with a modified methodology that takes into consideration the above link-melting phenomenon.

The algorithm was applied twice for each of the four tests. The first application involved experimental data from the initiation of the test up to the time, $t = t_{\text{MELT}}$, when the measured link temperature, T_1 , reaches the plateau, close to $T_{\text{FUSE}} = 74^\circ\text{C}$, that clearly indicates initiation of the link-melt process. Note that in this $0 \leq t \leq t_{\text{MELT}}$ time interval, the original equation set is still expected to represent a valid model, since the objections raised earlier regarding phenomenon of solder melting has not yet been initiated. As can be seen in Figs. 6–9, there is no ambiguity in choosing the experimental time and corresponding T_i sets that correspond to $t = t_{\text{MELT}}$. For each test, define N_M as the number of times that data were acquired up to t_{MELT} . Values of t_{MELT} and N_M are included in Table 2.

For each of the tests, the second application of the algorithm involved all of data in the interval $0 \leq t \leq t_{\text{FUSE}}$.

11.2. An initial estimate of the system parameters

The essential subroutine of the algorithm software is *SNLSIE*. To use this, it is necessary to provide as input an initial estimate of the system parameters. Based on Eqs. (8), the geometry of the elements, their material properties, measurements of their masses ($m_1 = 0.0156$ kg; $m_2 = 0.0280$ kg; $m_3 = 0.780$ kg), and using Eqs. (13) and (14),

Table 3

System parameters determined from the least-squares curve fitting algorithm (all ε 's of Eq. (18) assumed to be 0.9)

	Fit from $t = 0$ to $t = t_{\text{MELT}}$				Fit from $t = 0$ to $t = t_{\text{FUSE}}$			
	Test number				Test number			
	1	2	3	4	1	2	3	4
$RTI_1(\text{ms})^{1/2} =$	83.01	76.53	88.16	71.96	66.58	65.54	102.5	52.17
$RTI_2(\text{ms})^{1/2} =$	100.1	46.40	15.45	NA	119.7	70.13	19.27	NA
$RTI_3(\text{ms})^{1/2} =$	1488	1907	1907	NA	1448	1547	2293	NA
$C_{12}(\text{ms})^{1/2} =$	1.401	1.684	0.8286	NA	3.334	3.060	6.370	NA
$C_{23}(\text{ms})^{1/2} =$	12.44	14.04	5.065	NA	13.83	13.41	4.409	NA
Total	0.0261	0.0296	0.0767	0.0340	0.0675	0.0584	0.0962	0.0880
Residuals/ $N =$								
Figure no.	10	11	12	13	14	15	16	17

an initial estimate for the parameters of the three-element link–mount assembly was determined to be the estimate of three-element link–mount parameters:

$$\begin{aligned} RTI_1 &= 200 (\text{ms})^{1/2}, RTI_2 = 430 (\text{ms})^{1/2}, RTI_3 = 777 (\text{ms})^{1/2}, \\ C_{12} &= 1.04 (\text{ms})^{1/2}, C_{23} = 7.7 (\text{ms})^{1/2}. \end{aligned} \quad (23)$$

11.3. The optimum “solution” parameters and corresponding simulated responses

Results of the above algorithm applications, i.e., the “best-fit” sets of values for the RTI_i and C_{ij} , are presented in Table 3. As indicated in the table, simulations for the test $T_i(t)$'s that correspond to these sets of values, i.e., the solutions to Eqs. (8''), (18) and (10''), are presented in Figs. 10–13 for the $0 \leq t \leq t_{\text{MELT}}$ data fits and in Figs. 14–17 for the $0 \leq t \leq t_{\text{FUSE}}$ data fits. Included in Figs. 10–17 are the applicable experimental data as were presented previously in Figs. 6–9.

As can be seen in Figs. 10–13, in the range $0 \leq t \leq t_{\text{MELT}}$ and for the $0 \leq t \leq t_{\text{MELT}}$ data fits, there is generally excellent agreement between the experimental data and the model simulations. Thus, for exposure to the particular plunge test environment of tests 1–4, and at least up to the initiation of link solder melting, the algorithm was successful in identifying sets of system parameters, the ones solved for and presented in Table 3 under the heading “fit from $t = 0$ to $t = t_{\text{MELT}}$ ”, that, when used with the model equation set Eqs. (8''), (18) and (10''), simulate well the measured response of the system configurations tested. Further, it is reasonable to expect that the same model equation set, with the same solution parameters of Table 3, but with arbitrary Eq. (10'')-conditions, will provide similarly accurate simulations for the system responses to arbitrary plunge test environments. Additional testing is required to determine if the latter expectation is realized. In response to the main objective of this work, it is finally expected that, when used with the general equation

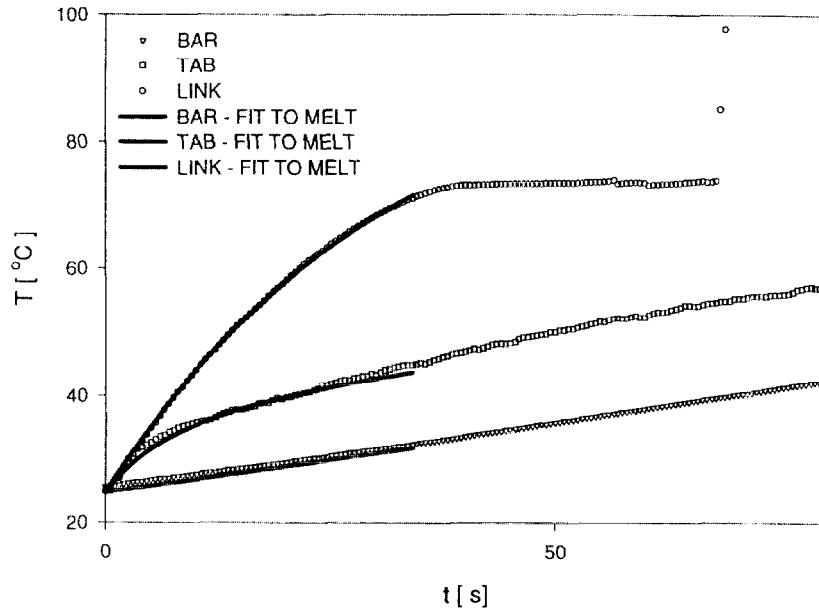


Fig. 10. Model simulation for the link-mount configuration and flow orientation of test 1 (see Tables 2 and 3), based on optimum fit to data from $t = 0$ to t_{MELT} .

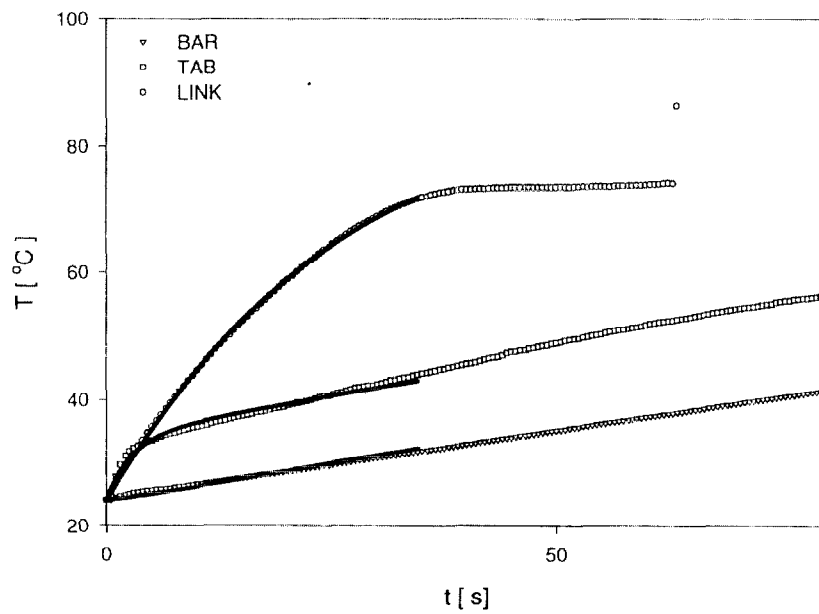


Fig. 11. Model simulation for the link-mount configuration and flow orientation of test 2 (see Tables 2 and 3), based on optimum fit to data from $t = 0$ to t_{MELT} .

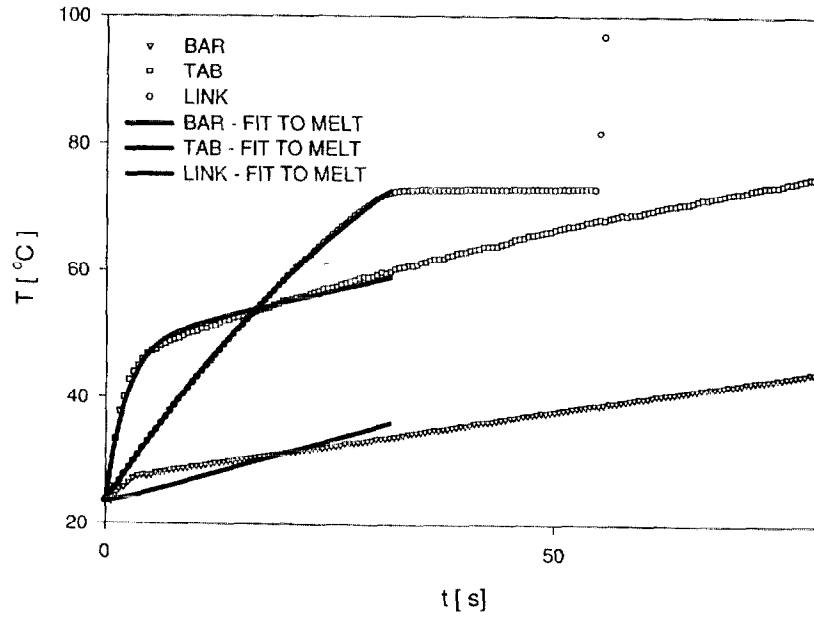


Fig. 12. Model simulation for the link-mount configuration and flow orientation of test 3 (see Tables 2 and 3), based on optimum fit to data from $t = 0$ to t_{MELT} .

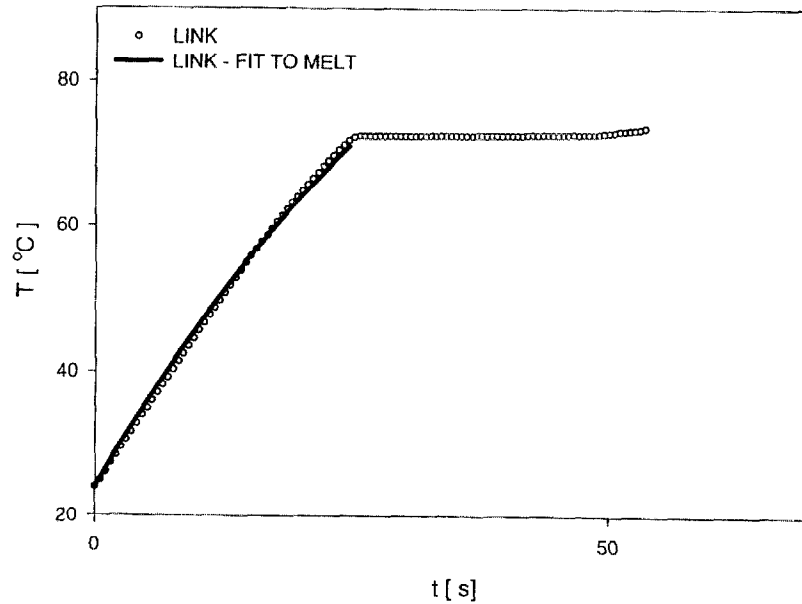


Fig. 13. Model simulation for the link-mount configuration and flow orientation of test 4 (see Tables 2 and 3), based on optimum fit to data from $t = 0$ to t_{MELT} .

set Eqs. (8''), (9), (10) and (12), the solution system parameters of Table 3 will lead to accurate simulations of the thermal response, in the range $0 \leq t \leq t_{\text{MELT}}$, of the configurations to arbitrary Eq. (10)-specified fire environments.

As can be seen in Figs. 10–13, in the range $0 \leq t \leq t_{\text{FUSE}}$, and in terms of predicting the critical event of system response, i.e., the time $t = t_{\text{FUSE}}$ when $T_1 = 74^\circ\text{C}$, the agreement between the experimental data and the model simulations is not good. In particular, in the figures and for the four tests, the predicted t_{FUSE} s are found to be 25–30% less than the corresponding measured t_{FUSE} s. Thus, as suggested earlier, for the fusible link design used in tests 1–4, and, no doubt, for other relatively large-solder-mass link designs, the governing equation for T_1 has to be modified so that it models adequately the near-constant- T_1 solder-melt phase of link response.

12. Modifying the model equations to account for the solder-melting phase of link response

12.1. Simulating the solder-melting phase of link response

For a link design with arbitrary specified T_{FUSE} , the near-constant- T_1 solder-melting phase of link response can be closely simulated by adding the following constraint to the model equations, Eqs. (8'') and (8'''):

$$\text{if } T_1 \geq T_{\text{FUSE}} \quad \text{then } dT_1/dt = 0. \quad (24)$$

Note from the first of the model equations, the ones for T_1 , and from Eq. (13), where it is seen that RTI_i is proportional to c_i , that the above constraint is equivalent to an assumed arbitrarily large step increase in c_i , in the temperature range $T_1 \geq T_{\text{FUSE}}$, from its specified constant low-temperature value. This increase in effective specific heat of the link simulates the action of the latent heat of melting of the solder, which maintains the entire link component at the nearly constant temperature, T_{FUSE} , as the solder absorbs the relatively large amount of energy required to bring it from a solid to liquid state.

With the Eq. (24)-modified model equations, the curve-fitting algorithm can be applied again, as above. The result would be sets of solution system parameters, to be used to revise Table 3 entries under the heading “fit from $t = 0$ to $t = t_{\text{FUSE}}$ ”.

It is clear from a visual inspection of the data, e.g., Figs. 14–17, that the revised model equations, used with the latter revised solution system parameters, would lead to improved goodness of fit between simulation and experiment, in the sense of reducing G of Eq. (20). However, with regard to providing an accurate simulation estimate for the critical value t_{FUSE} , the situation is far worse than before. Thus, while the original simulation estimates for t_{FUSE} were 25–30% less than the measured values, the revised model equations, i.e., with the constraint of Eq. (24), do not yield *any* unique prediction of t_{FUSE} !

To resolve the situation, additional modeling detail of the solder-melting process is required. In this regard, a variety of different modeling approaches are possible, e.g., an approach where the model accounts for time-dependent changes of m_i due to loss

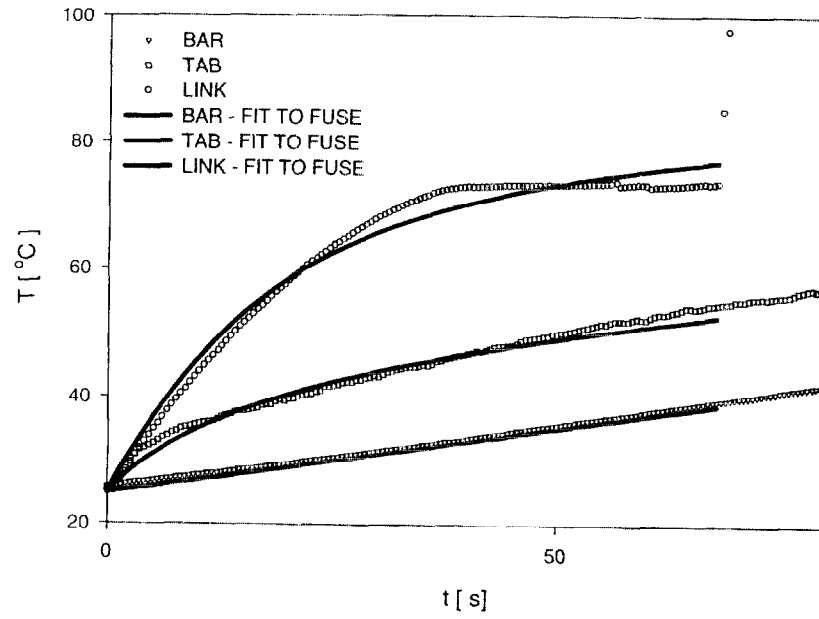


Fig. 14. Model simulation for the link-mount configuration and flow orientation of test 1 (see Tables 2 and 3), based on optimum fit to data from $t = 0$ to t_{FUSE} .

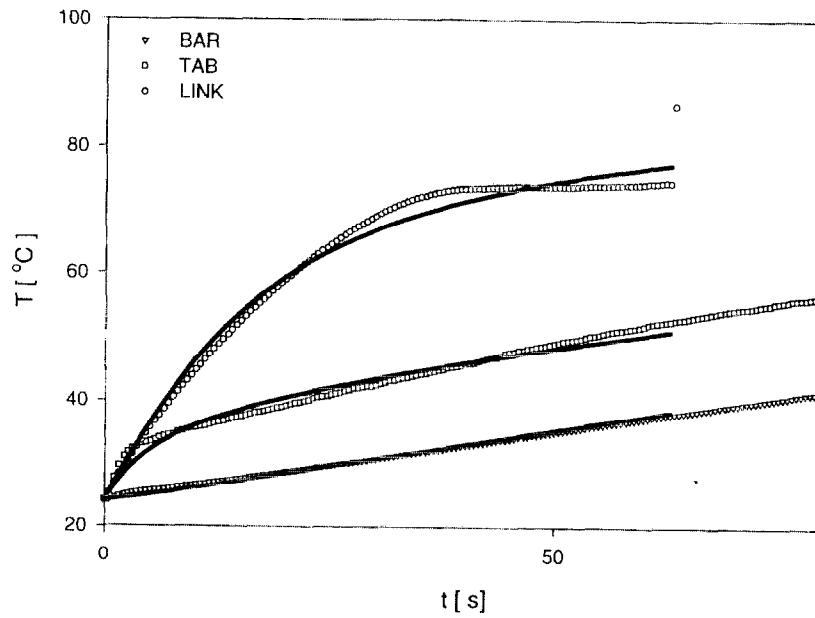


Fig. 15. Model simulation for the link-mount configuration and flow orientation of test 2 (see Tables 2 and 3), based on optimum fit to data from $t = 0$ to t_{FUSE} .

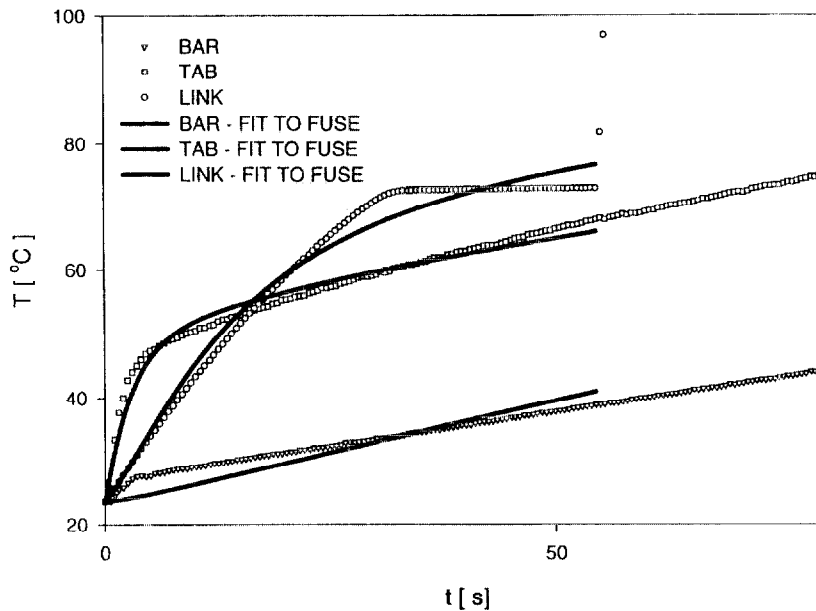


Fig. 16. Model simulation for the link-mount configuration and flow orientation of test 3 (see Tables 2 and 3), based on optimum fit to data from $t = 0$ to t_{FUSE} .

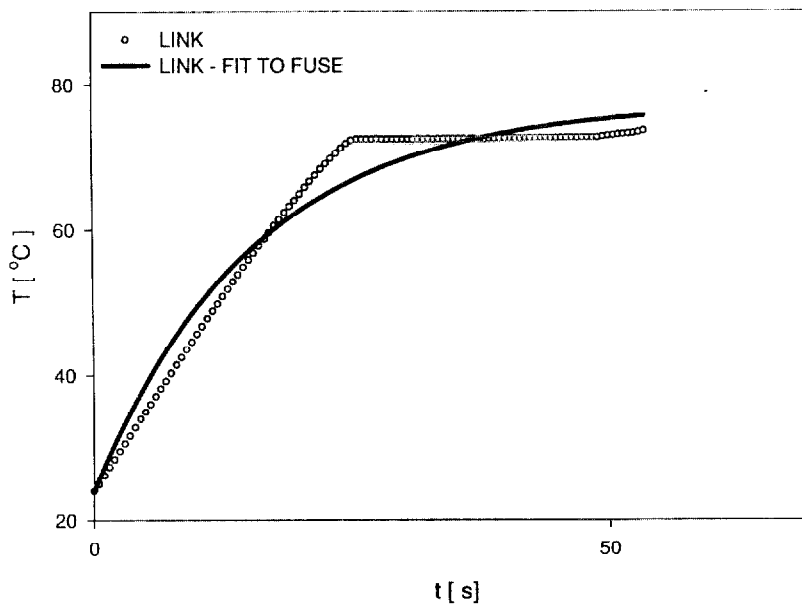


Fig. 17. Model simulation for the link-mount configuration and flow orientation of test 4 (see Tables 2 and 3), based on optimum fit to data from $t = 0$ to t_{FUSE} .

of solder (dripping) during the melting process. (In general, the mass of the pre-melt solder component of the link can be a significant fraction of m_1 .) However, to achieve the stated objective of this work it seems that an elaborate analysis is unnecessary.

12.2. The seven-step procedure for determining system parameters and establishing final model equations

Consistent with the above results and ideas, an alternative variation to the Eq. (24)-approach will now be presented that yields a general model for simulating the thermal response, including a prediction for t_{FUSE} , of any particular three-element link–mount system configuration.

Values for the system parameters are determined and the final model equations are established by carrying out the following steps, referred to below as the “seven-step procedure”:

1. Acquire plunge test data for the system configuration to be modeled, similar to the data of tests 1–4, where the configuration includes a particular fusible link design with manufacturer-specified T_{FUSE} . From the data, identify the value of t_{FUSE} .
2. Using the curve fit algorithm, determine system parameters RTI_i and C_{ij} associated with the solution to the model equations, Eqs. (8''), (18), (10'') and (24), that yields a best fit to the data in the range $0 \leq t \leq t_{\text{FUSE}}$. In the latter implementation of the algorithm, the values of all ϵ 's of Eq. (18) are assumed to be known and specified. (For results reported in this work, all ϵ 's were always specified as 0.9.)
3. Consistent with the plunge test data, select a relatively-small (compared to $\Delta T = T_{\text{FUSE}} - T_{\text{AMB}}$) temperature increment, ΔT_{MELT} , such that the relatively constant-temperature solder-melt region of the T_1 data of the test of item 1 are in the range $T_{\text{FUSE}} - \Delta T_{\text{MELT}} \leq T_1 \leq T_{\text{FUSE}}$.
4. Define the solid-to-liquid phase change of the link solder as being initiated at temperature T_{MELT} , where

$$T_{\text{MELT}} = T_{\text{FUSE}} - \Delta T_{\text{MELT}}. \quad (25)$$

From the experimental data, identify the time t_{MELT} , when T_1 first reaches T_{MELT} .

5. Define RTI_{MELT} as the new, effective, melt-phase value of RTI_1 , to be determined below. (This will have the property: $\text{RTI}_{\text{MELT}} \gg \text{RTI}_1$.) Corresponding to RTI_{MELT} is c_{MELT} , the newly defined, effective, melt-phase value of c_1

$$c_{\text{MELT}} \equiv c_1 \text{RTI}_{\text{MELT}} / \text{RTI}_1. \quad (26)$$

Add the following constraint to the model equations:

$$\begin{aligned} \text{if } T_{\text{MELT}} \leq T_1 \leq T_{\text{FUSE}}, \quad \text{then, in Eqs. (8''), (12), and (18), replace } \text{RTI}_1 \\ \text{by } \text{RTI}_{\text{MELT}} \text{ and } c_1 \text{ by } c_{\text{MELT}}. \end{aligned} \quad (27)$$

6. Find the value of RTI_{MELT} that leads to a solution to Eqs. (8''), (18), (10'') and (27), integrated in the range $0 \leq t \leq t_{\text{FUSE}}$, that satisfies the condition

$$T_1(t_{\text{FUSE}}) = T_{\text{FUSE}}. \quad (28)$$

Designate this value of RTI_{MELT} as a new fixed system parameter, in addition to the RTI_i and C_{ij} determined above in item 4.

7. The final model equations are: Eqs. (8''), (9), (12), (10) and (27), for fire scenarios; or, in the case of tunnel test simulations: Eqs. (8''), (18), (10'') and (27). In general applications of the model, fusing of the link is predicted to occur at the first simulated time when $T_1 = T_{\text{FUSE}}$.

In the above procedure, step 2 insures a good fit between model simulation and experimental data, while step 6 insures that, in the temperature range of solder melting, while the link passes through the (relatively small) temperature increment ΔT_{MELT} immediately prior to T_{FUSE} , the effective specific heat of the link is significantly increased to the value that provides the amount of latent heat, $m_{\text{MELT}}L_{\text{MELT}}$, to melt the exact amount of solder, m_{MELT} required to fuse the link, i.e., where

$$c_1(T) = c_{\text{MELT}}, T_{\text{MELT}} - \Delta T_{\text{MELT}} \leq T \leq T_{\text{MELT}},$$

$$L_{\text{MELT}} = \int_{T_{\text{MELT}} - \Delta T_{\text{MELT}}}^{T_{\text{MELT}}} c_{\text{MELT}} dT = c_{\text{MELT}} \Delta T_{\text{MELT}}. \quad (29)$$

It is of interest to note that the use of a relatively large effective value of link specific heat, in step 6, for simulating the effect of melting of the link's solder on link thermal response is analogous to the use in Refs. [19,20] of a similarly large effective specific heat for simulating the effect of evaporation of free water over a small temperature interval on the thermal response of fire-exposed gypsum wall board.

The above approach assumes that in any relevant scenario, once $T_1(t)$ exceeds T_{MELT} it continues to increase monotonically with t . Additional considerations, beyond the scope of this present work, can lead to modification to the final model equations so that they can be used to simulate scenarios where the link is: heated to the point of sustained melting, with loss of some, but not all of its solder; cooled; reheated to the melt condition, etc.

12.3. Using the plunge test data for a final determination of system parameters for the Table 2 configurations

The seven-step procedure was carried out for the plunge test data and corresponding system configurations of test 1–4, with $T_{\text{FUSE}} = 74^\circ\text{C}$ and $\Delta T_{\text{MELT}} = 2^\circ\text{C}$. The results are presented in Table 4. As indicated in the table, plots of the final model simulation are presented in Figs. 18–21, corresponding to tests 1–4, respectively.

As can be seen from Figs. 18–21, the solutions to the final model equations, with system parameters determined according to the seven-step procedure, yield simulations that provide excellent matches with the data of tests 1–4. Note that in the simulations, when T_1 , the link temperature, reaches T_{FUSE} , the vent is predicted to open automatically, and no physical significance is attached to subsequent (relatively rapid rates-of-rise of) predicted values of T_1 .

Although the $T_i(t)$ responses of the essentially identical link-mount configurations in tests 1 and 2 are closely reproduced, and this in spite of the different flow

Table 4

System parameters determined according to the seven-step procedure for the system configurations and the data of tests 1–4 (see Table 2) with $T_{\text{FUSE}} = 74 \text{ C}$ and $\Delta T_{\text{MELT}} = 2 \text{ C}$

	Fit from $t = 0$ to $t = t_{\text{FUSE}}$			
	Test number			
	1	2	3	4
$RTI_1/(\text{ms})^{1/2} =$	93.71	74.96	94.56	71.62
$RTI_2/(\text{ms})^{1/2} =$	160.0	76.64	19.26	NA
$RTI_3/(\text{ms})^{1/2} =$	1279	1507	2377	NA
$C_{12}/(\text{ms})^{1/2} =$	0.2581	2.057	2.375	NA
$C_{23}/(\text{ms})^{1/2} =$	7.732	12.30	4.434	NA
Total residuals/ $N =$	0.0385	0.0383	0.0787	0.0359
$RTI_{\text{MELT}}/(\text{ms})^{1/2} =$	1681	671.4	840.0	1457
Figure no.	18	19	20	21

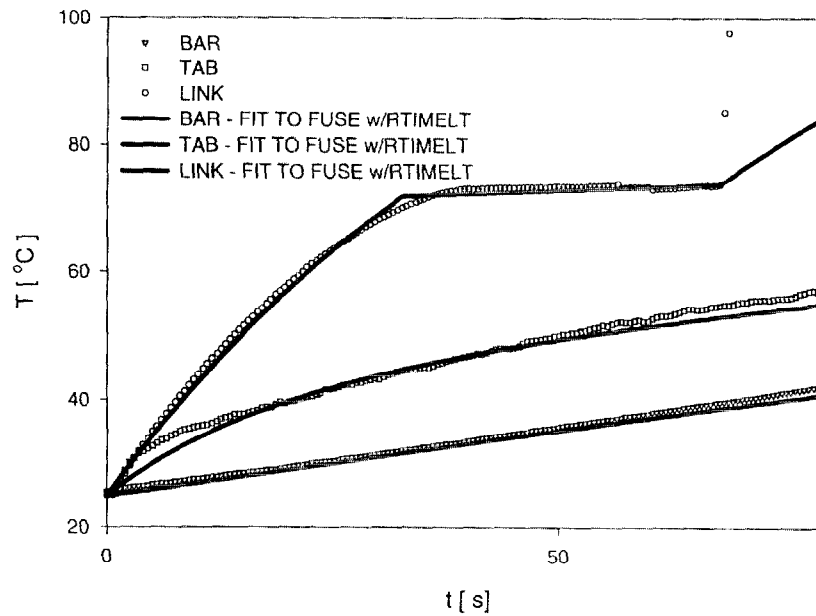


Fig. 18. Model simulation based on the seven-step procedure for the link-mount configuration and flow orientation of test 1 (see Tables 2 and 4).

orientations, the solution system parameters for these test are significantly different, e.g. in Table 4, compare the RTI_1 s (93.71 and 74.96), the RTI_2 s (0.2581 and 2.057), and the RTI_{MELT} s (1681 and 671.4). Nevertheless, although there is a difference in the predicted critical value of t_{FUSE} (68.0 vs. 63.0 s), corresponding properly to the measured values as reported in Table 2, the solution of the model equations for

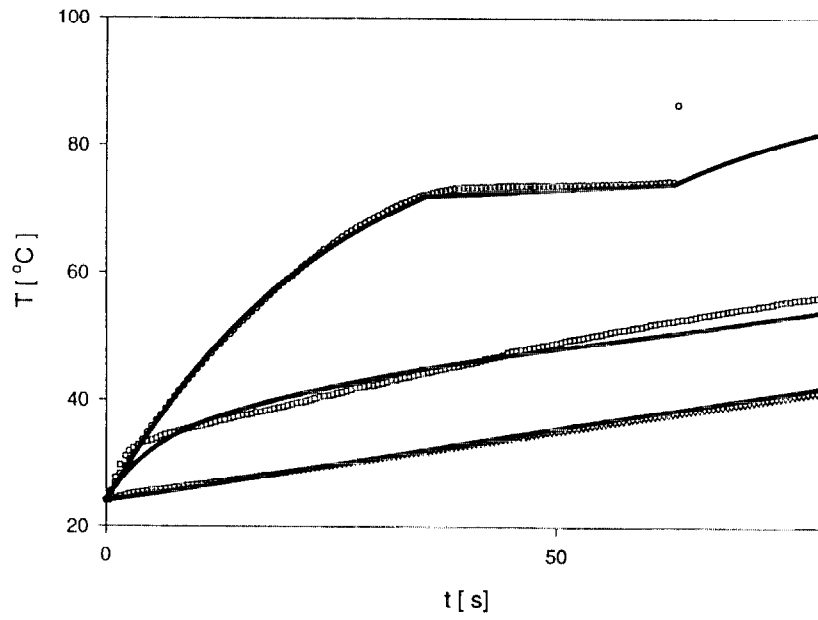


Fig. 19. Model simulation based on the seven-step procedure for the link-mount configuration and flow orientation of test 2 (see Tables 2 and 4).

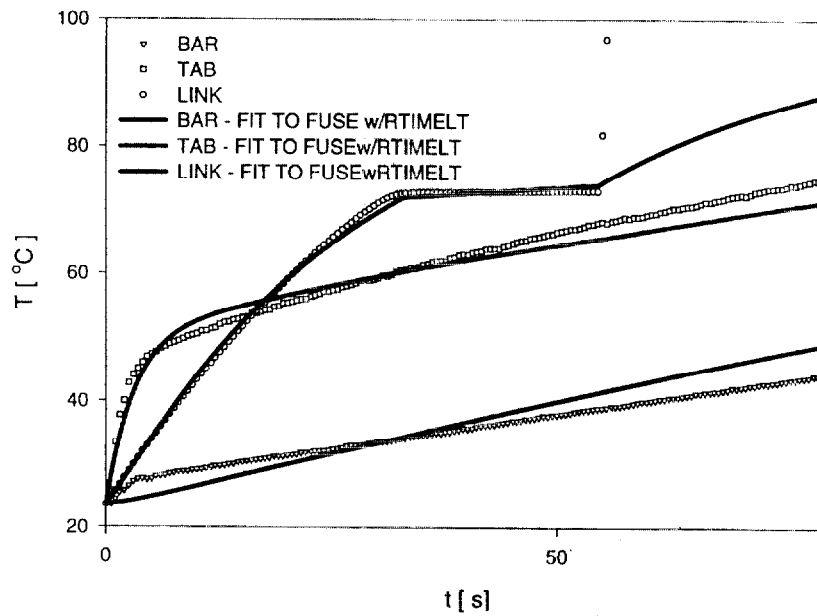


Fig. 20. Model simulation based on the seven-step procedure for the link-mount configuration and flow orientation of test 3 (see Tables 2 and 4).

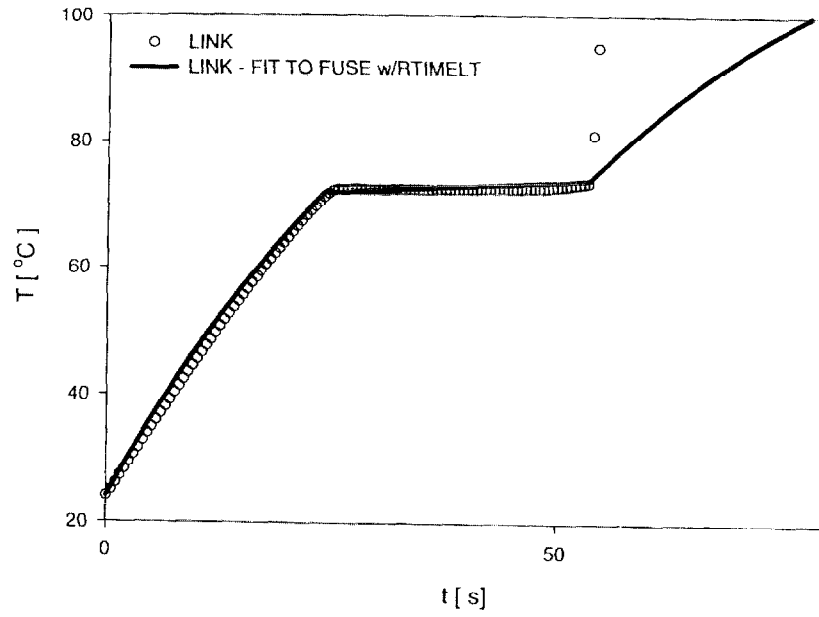


Fig. 21. Model simulation based on the seven-step procedure for the link-mount configuration and flow orientation of test 4 (see Tables 2 and 4).

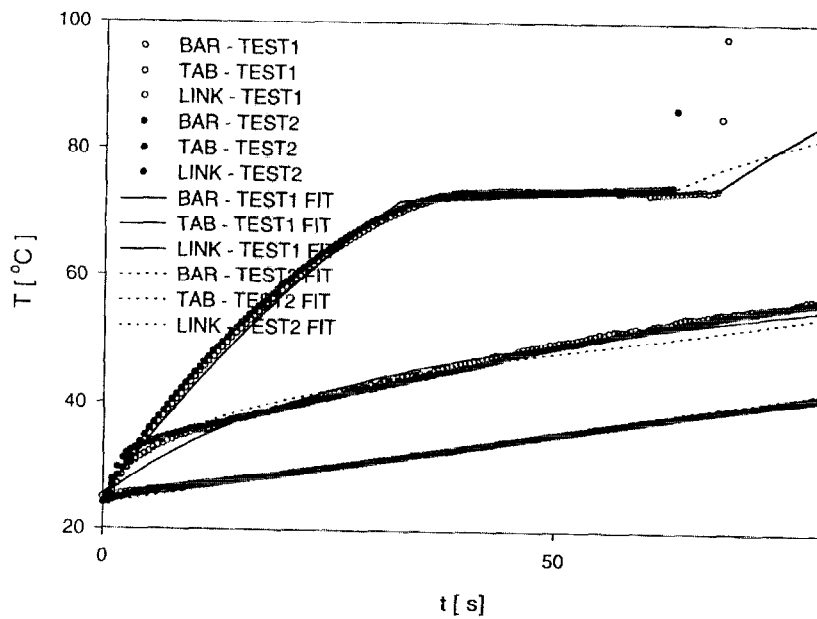


Fig. 22. Model simulations based on the seven-step procedure for the link-mount configurations and flow orientations of tests 1 and 2 (see Tables 2 and 4).

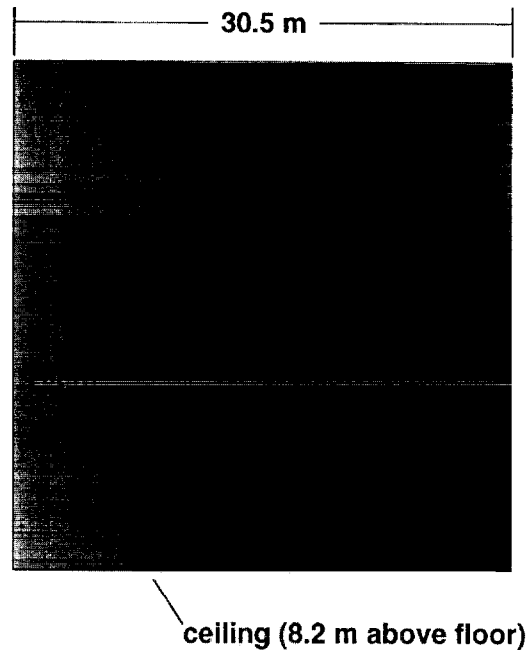


Fig. 23. Sketch of fire scenario for the large-scale two-vent test of Ref. [10].

the set of system parameters derived from either one of the tests provides good matches to the experimental data of the other. This is illustrated in Fig. 22, where the experimental data and the model simulations of both tests 1 and 2 are all plotted together.

13. An example application and validation of the model equations

13.1. Measured response of the three-element link-mount in a real fire scenario

This section uses the model equations, developed to characterize the three-element link-mount system of tests 1 and 2, to simulate the measured response of this same link-mount system, used in the vent design of one test fire scenario reported in Ref. [10].

Refer to Fig. 23. The fire scenario involved a $1.01 \text{ m} \times 1.01 \text{ m}$ square heptane spray burner located 0.61 m above the floor in a facility with a flat square ($30.5 \text{ m} \times 30.5 \text{ m}$) unconfined ceiling. The facility was identical to the one used in the tests of Refs. [7–9]. There it was indicated that the lower exposed ceiling surface was made up of 0.0159 m -thick insulating tiles with specific heat $753 \text{ J}/(\text{kg K})$, thermal conductivity $0.0611 \text{ W}/(\text{m K})$, and density $313 \text{ kg}/\text{m}^3$. The ceiling-to-floor spacing was 8.2 m . The vents were $1.22 \text{ m} \times 2.44 \text{ m} \times 0.30 \text{ m}$ (depth). They were mounted in the ceiling with centers spaced at 6.10 m and symmetrically placed relative to the vertical axis of the

burner, i.e., the radius from the burner axis to the center of a vent was 3.05 m. Relative to the axis of the fire and the radial flow in the ceiling jet, the orientation of the link-mount system was as in Fig. 2, with expected parallel system/flow orientation as in test 2 (refer to Table 2).

The flow of fuel to the burner was controlled to yield a total fire energy release rate of

$$\dot{Q}_{\text{FIRE}} = \begin{cases} 10^5 [t/(75 \text{ s})] \text{ kW}, & 0 \leq t < 75 \text{ s}, \\ 10^5 \text{ kW}, & 75 \text{ s} \leq t. \end{cases} \quad (30)$$

The fire was extinguished at 150 s.

In the experiment, the link of the west vent fused and the vent opened at $t = 90$ s. During the test, the east vent link did not fuse and the vent did not open. (As indicated by thermocouple data near the vents, the failure of the east vent to open can be explained by the fact that, upon opening of the west vent, the fire plume tilted immediately toward the west. As a result of this, the ceiling jet velocity and temperature in the vicinity of the east vent were reduced from their peak values and the temperature of its link never achieved T_{FUSE} .)

13.2. Simulated response of the links

To use the model equations to simulate the response of the links in the above experiment, it was necessary to estimate $u(t)$, $T_G(t)$, and $T_{\text{CEIL}}(t)$. This was accomplished with the use of the fire model *LAVENT* [6,13,14].

The three-element link mount, including the link itself is within the vent cavity, the depth of which is 0.30 m. During the fire scenario, as the turbulent ceiling jet flows past the vent cavity it would “fill” the cavity with a turbulent flow having the same local characteristic velocities and temperatures. It is expected that the characteristics of the cavity flow and, in particular, the values of $u(t)$ and $T_G(t)$ local to the link, are related to the velocity and temperature, respectively, of an undisturbed ceiling jet that would exist in the absence of vent deployment. Here it is assumed that $u(t)$ and $T_G(t)$ are equal to the velocity and temperature, respectively, of this undisturbed ceiling jet, averaged from the ceiling surface and down to the depth equal to the depth of the vent, 0.30 m in the present scenario.

From the above considerations and test parameters, the specified time-dependent conditions of Eq. (10), necessary to solve the model equations, Eqs. (8’), (9), (12) and (27) were determined. These are plotted in Fig. 24.

The model equations were solved using the system parameters, as listed in Table 4, determined from both tests 1 (normal flow) and 2 (parallel flow). The solutions resulted in t_{FUSE} estimates of 72.5 and 81.0 s. These are to be compared to the experimentally measured result of 90 s. As mentioned, of the two system characterizations, the one from test 2, for parallel flow, which led to the $t_{\text{FUSE}} = 72.5$ s estimate, is expected to correspond more closely to the system as deployed in the particular test under discussion.

The differences between measured and predicted values of t_{FUSE} can be attributed mainly to differences between the actual vs expected history of \dot{Q}_{FIRE} as specified in

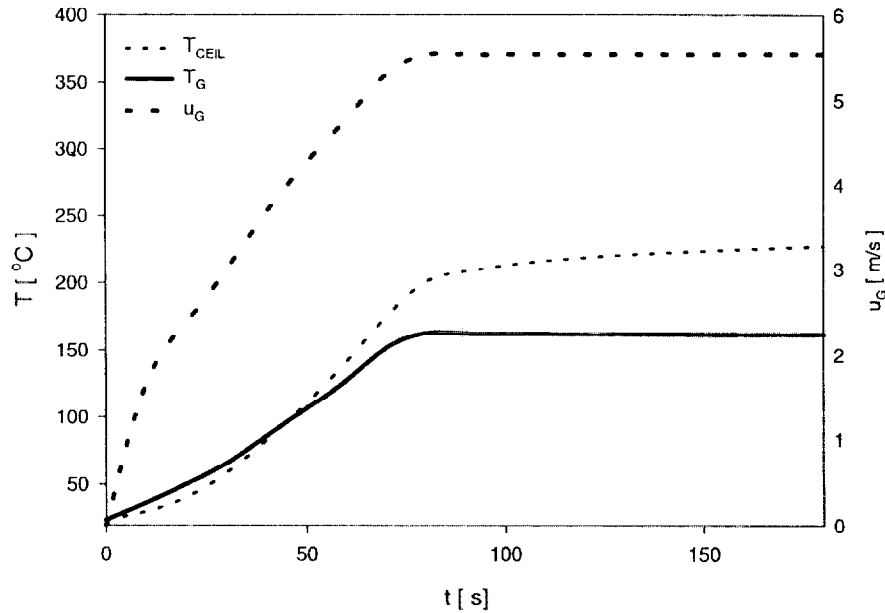


Fig. 24. Simulation of $T_G(t)$, $u(t)$, and $T_{CEIL}(t)$ during the test of Ref. [10] local to the three-element vent link-mounts.

Eq. (30). Near-ceiling thermocouple data reported for the present test [10], and for other tests with \dot{Q}_{FIRE} specified as in Eq. (30), indicate that in the early several tens of seconds of these tests, it is reasonable to expect time shifts in $\dot{Q}_{FIRE}(t)$, i.e., delays of the order of 10–20 s (see Figs. 9–11 of Ref. [10]), leading to corresponding time delays in the expected response of link/vent activation.

14. Summary and conclusions

Model equations, suitable for general use in compartment fire models, were developed [Eqs. (8''), (9), (12), (10) and (27)] to simulate the thermal response to arbitrary fire environments of fusible-link-actuated fire vents. The method of analysis, which focused on a prototype three-element link-mount design, can be extended to arbitrary multiple-element link mounts. Also, the equations for the prototype three-element link mount were shown to include, and be directly applicable to the problem of simulating the response of single-element simply supported links.

A method was developed to determine the values of the set of parameters that characterize a particular multiple link-mount design; five parameters in the case of the above three-element link mount. This involves: (1) the measured time-dependent thermal response of the link-mount design to exposure in a plunge test, the type of test

used to characterize the thermal response of sprinkler links; and (2) an analytic means of determining values of the design parameters that yield an optimum fit between a solution to the model equations and the temperature data. The method was presented in an earlier section of this work entitled “*A Seven-Step Procedure for Determining System Parameters and Establishing Final Model Equations*”.

In developing the model equations within the context of plunge test results, it was determined from the measured temperature–time responses of the links that, for the particular link design used in the present tests, and, no doubt, for other relatively large-solder-mass-link designs, the time interval over which link-solder melting takes place (i.e., the interval, prior to fusing, during which time the link temperature remains close to its fuse temperature) is a significant fraction of the total time to fuse. For this reason, and in contrast to the traditional way of modeling the response of fusible links which, in the case of links used in sprinkler designs has proven to be very robust, it was concluded that model equations must account for the solder-melt phenomenon. Such an accounting is included in the *seven-step procedure*.

The *seven-step procedure* was carried out successfully for four plunge tests involving three link–mount systems and one or two system/flow orientations. In each case, the determined values of the system parameters with the model equations lead to excellent simulations of the plunge test data. The resulting system parameters and model equations corresponding to the three-element link mount design of the fusible-link vent test of Ref. [10] were used successfully to simulate time of link fusing and vent activation in a large-scale heptane-spray-burner fire environment.

Although the experimental results from both the plunge tests and the large-scale test support strongly the proposed mathematical model for link assembly thermal response and the proposed experimental procedure for determining link assembly characteristics, the ideas presented in this work should be subjected to significant additional testing before being adopted for general use.

Acknowledgements

All tests reported in this work, including the design, assembly, and instrumentation of all test fixtures, were carried out by Mr. A. Jay McElroy. All data reduction was carried out by Mr. David Stroup. The author acknowledges gratefully the support of both of these gentlemen.

References

- [1] Heskestad G, Smith HF. *Investigation of a new sprinkler sensitivity approval test: the plunge test*, FMRC 22485. Factory Mutual Research Corporation, Norwood, MA, 1976.
- [2] Heskestad G, Smith HF. *Plunge test for the determination of sprinkler sensitivity*, FMRC 3A1E2.RR. Factory Mutual Research Corporation, Norwood, MA, 1980.
- [3] Evans DD, Madrykowski D. *Characterizing the thermal response of fusible-link sprinklers*, NBSIR 81-2329. National Institute of Standards and Technology (formerly National Bureau of Standards), Gaithersburg MD, August 1981.

- [4] International Organization for Standardization (ISO). Fire protection — automatic sprinkler systems Part I: requirements and test methods for sprinklers, ISO 6182-1. Geneva, Switzerland, 1993.
- [5] Evans DD. Calculating sprinkler actuation times in compartments. *Fire Safety Journal* 1985;9: 147–55.
- [6] Cooper LY. Estimating the environment and the response of sprinkler links in compartment fires with draft curtains and fusible link-actuated ceiling vents: theory. *Fire Safety Journal* 1990;16:137–63.
- [7] Sheppard DT, Steppan DR. Sprinkler, heat & smoke vent, draft curtain project — Phase 1 scoping tests. Technical Report. Underwriters Laboratories, Inc., Northbrook IL, May 1997.
- [8] Sheppard DT. International fire sprinkler, heat & smoke vent, draft curtain fire test project — Test Report, Technical Report NC987-96NK37863. Underwriters Laboratories, Inc., Northbrook IL, 1998.
- [9] McGrattan KB, Hamins A, Stroup D. Sprinkler, smoke & heat vent, draft curtain interaction — large scale experiments and model development, NISTIR 6196-1. National Institute of Standards and Technology, Gaithersburg MD, September 1998.
- [10] Sheppard DT. Sensitivity of roof mounted heat and smoke vents. Test Report prepared for Industrial Risk Insurers and Conspec Systems, Inc. by Underwriters Laboratories, Northbrook IL, January 9, 1998.
- [11] Eckert ERG, Drake RM. Heat and mass transfer. New York: McGraw-Hill, 1959.
- [12] Ražnjević K. Handbook of thermodynamic tables and charts. Washington, DC: Hemisphere, 1975, p. 309.
- [13] Davis WD, Cooper LY. Estimating the environment and the response of sprinkler links in compartment fires with draft curtains and fusible link-actuated ceiling vents — Part II: User guide for the computer code LAVENT, NISTIR 89-4122. National Institute of Standards and Technology, Gaithersburg MD, August 1989.
- [14] LAVENT. Appendix B: The theoretical basis of LAVENT, and Appendix C: user guide for the LAVENT computer code. NFPA 204 Guide for smoke and heat venting. 1998 ed., NFPA, Quincy, MA, 1998.
- [15] Heskestad G, Bill RG. Quantification of thermal responsiveness of automatic sprinklers including conduction effects. *Fire Safety Journal*, 1988;14:113–25.
- [16] Heskestad G, Bill RG. Modeling of thermal responsiveness of automatic sprinklers. *Fire Safety Science* — Proceedings of the Second International Symposium, IAFSS, Hemisphere, 1989, pp. 603–612.
- [17] Press WH, Flannery BP, Teukolsky SA, Vetterling WT. Numerical recipes — the art of scientific computing. Cambridge, 1986.
- [18] Hiebert KL. Fortran subroutine SNLSIE, to minimize the sum of squares of M nonlinear functions in N variables (from subprogram library CMLIB). Sandia National Laboratory, Albuquerque NM, 1984.
- [19] Mehalley JR, Cuerrier P, Carisse G. A Model for predicting heat transfer through gypsum-board/wood-stud walls exposed to fire. *Fire and Materials* 1994;18:297–305.
- [20] Cooper LY. The thermal response of gypsum-panel/steel-stud wall systems exposed to fire environment — a simulation for use in zone-type fire models, NISTIR 6027. National Institute of Standards and Technology, Gaithersburg MD, June 1997.